PHYSICAL REVIEW D VOLUME 9, NUMBER 6 15 MARCH 1974

Crystallization of dense neutron matter

V. Canuto*
Institute for Space Studies, Goddard Institute for Space Studies, NASA, New York, New York 10025

S. M. Chitre†
Belfer Graduate School of Science, Yeshiva University, New York, New York 10033
(Received 25 May 1973; revised manuscript received 12 October 1973)

The equation of state for cold neutron matter at high density is studied in the t-matrix formulation and it is shown that energetically it is convenient to have neutrons in a crystalline configuration rather than in a liquid state for values of the density exceeding 1.6×10^{15} g/cm^3. The study of the mechanical properties indicates that the system is stable against shearing stresses. A solid core in the deep interior of heavy neutron stars appears to offer the most plausible explanation of speed-ups observed in the Vela pulsar.

I. INTRODUCTION

The discovery of pulsars and their plausible identification with rotating neutron stars has led to a considerable interest in the physics of neutron stars, particularly with regard to the equation of state governing matter at high densities. A large number of equations of state have been constructed at zero temperature and it is only fair to say that the state of matter appears to be reasonably well understood up to the nuclear density ($\rho\simeq3\times10^{14}$ g/cm^3). A comprehensive review of the equation of state up to this density and above this density may be found in the review articles of Wheeler,[1] Cameron,[2] and Canuto.[3] As a result of the large variation of the density from the surface through the center, the structure of a neutron star is composed of layers with different physical characteristics. What makes the study of these stars so fascinating is that the physical conditions prevailing in their interior provide an ideal testing ground for theories of nuclear and neutron matter. The observed pulsar speed-ups[4] has also presented an interesting test for the model calculation of neutron stars.

The original structure calculation of Oppenheimer and Volkoff[5] treated the interior of a neutron star as a noninteracting Fermi gas and this yielded an upper limit of $0.7M_\odot$ for a stable neutron star. The model calculations were later improved by Tsuruta and Cameron[6] by incorporating the effects of the nuclear forces among the particles and this naturally raised the upper limit of a stable neutron star to about $2M_\odot$. The exact value of the upper limit is, however, subject to a considerable amount of uncertainty, because in the model calculations the density at the maximum occurs at densities around 10^{15} g/cm^3, and this involves an extrapolation of the many-body techniques to a region substantially above the nuclear density. There was in fact no reliable calculation available in the density range $10^{15}\leq\rho\leq10^{16}$ g/cm^3 as can be seen from the results of Tsuruta and Cameron[6] which gave significantly different mass limits upon using Levinger and Simmons's velocity-dependent potentials V_β and V_γ. This prompted Banerjee, Chitre, and Garde[7] to adopt, following a suggestion by Bethe, an approach which assumes that when the nuclear forces become sufficiently repulsive a possible minimum energy state can be achieved by keeping the nucleons as far away from one another as possible, i.e., by localizing them at lattice sites. Such a solid lattice of neutrons would be a nuclear analog of the Coulomb lattice of nuclei which exists in the outer crust of a neutron star. The lattice calculation was performed with the harmonic approximation using the classical Debye model and employing a Reid soft-core potential for the interaction among neutrons. It was found that the lattice was stable in the density regions upwards of 8×10^{14} g/cm^3, but the resulting energy per particle could not be compared with any existing computation as there was no calculation available which was done in the same spirit, and in that sense the result was inconclusive.

Shortly afterwards Pandharipande[8] calculated the binding energy per particle of a neutron liquid up to a density of 4 neutrons/fm^3 using the Reid soft-core potential. In Pandharipande's lowest-order variational formulation, the trial wave function is expressed as a product of single-particle wave functions and the short-range calculation in the manner of Jastrow. A differential equation for the correlation function is then derived by minimizing the energy with a constrained variation. The energy, which is calculated using clusters up to two bodies, was found to be lower by a factor

of two compared with the energy computed by Banerjee *et al.* in the density range $7.5\times10^{14} \leq \rho \leq 6\times10^{15}$ g/cm^3. This immediately demonstrated the need for a quantum-mechanical computation of the neutron lattice which is expected to lower the energy in relation to the classical Debye calculation by spreading the wave function around each lattice site thereby collecting more attraction in the final energy values. Moreover, the classical harmonic-oscillator treatment is hardly adequate for a satisfactory description of a neutron lattice which is a highly quantum crystal in the sense that the zero-point energy of the neutrons is comparable with the potential energy and the amplitude of oscillation becomes a sizable fraction of the interparticle distance.

There have been semiempirical attempts to study the possibility of crystallization of neutron matter especially from the point of view of determining the solidification pressure. Anderson and Palmer[9] were the first to appeal to de Boer's law of corresponding states by making use of empirical data regarding nuclear and neutron matter. They obtained a solidification density for neutron matter in the vicinity of 5×10^{14} g/cm^3, a result which was not significantly altered by a later refined version by Clark and Chao[10] who adapted an average Reid potential to a Lennard-Jones shape. This evidently raises a crucial question whether a neutron star may have a crystalline structure throughout its interior—a consideration which is of prime importance from the point of view of the dynamics of a neutron star. The argument based on the law of corresponding states cannot be taken literally insofar as its numerical predictions are concerned. Nevertheless, it gives a good physical insight into the nature of the problem. More specifically, it emphasizes the numerical equality (~3) of the de Boer parameter for solid ^{3}He and for a neutron lattice, and provides a semiquantitative answer to the question concerning the solidification of neutron matter under a sufficiently high pressure.

The present computation to study cold neutron matter is based on the t-matrix approach which has been successfully employed to describe the physical properties of quantum crystals like ^{3}He and ^{4}He. Our experience has been that since nuclear forces are highly spin- and angular-momentum-dependent, they cannot be easily incorporated in a variational method. In our approach we have managed to avoid a number of approximations which are usually invoked in the context of ^{3}He and have been able to bring out a full dependence of the wave function on spin and angular momentum. The principal feature of our work is that we find the onset of a solid phase for cold neutron matter in the density range upwards of 1.6×10^{15} g/cm^3. Recently there have been some more attempts to investigate the problem of the crystallization of dense neutron matter. Coldwell,[11] using orthogonal single-particle wave functions finds crystallization at a density of 7.78×10^{14} g/cm^3. Nosanow and Parish,[12] using a Monte Carlo technique analogous to the one used for solid ^{3}He, found the onset of a neutron solid at a density of 4.2×10^{14} g/cm^3; Schiff[13] using a fermion version of the quantum perturbation method developed by Kalos, Levesque, and Verlet estimated the crystallization density for cold neutron matter at $(2.9\pm0.5)\times10^{15}$ g/cm^3, while Pandharipande's[14] constrained variational computation yielded no solidification up to a density of 2 neutrons/fm^3.

The remainder of the paper is arranged as follows. In Sec. II we set out the mathematical formulation as applicable to a neutron lattice and in Sec. III we derive the general expressions for energy per particle interacting via a soft-core nucleon-nucleon potential. The self-consistent method for determining the frequency of oscillation for a neutron oscillating around a lattice site is described in Sec. IV and the various spin configurations of neutrons in a conventional lattice structure is set out in Sec. V. The elasticity of baryonic lattices is discussed in Sec. VI and the main thrust of our computation and the related problems with uncertainties of interaction potentials are discussed in Sec. VII. Finally the results are summarized in Sec. VIII along with a comparison with other neutron solid calculations and the astrophysical aspects are detailed in Sec. IX. A short version of this paper has appeared as a letter.[15]

II. GENERAL THEORY

It is customary to think of a crystal as an ordered array of particles oscillating about their mean lattice positions with amplitude small compared to the interparticle distance. Such a crystal can be adequately described by classical dynamics in the framework of the harmonic approximation. However, quantum crystals, such as solid helium, cannot be treated on the basis of classical lattice dynamics. This is largely a consequence of the fact that the attractive part of the interaction is quite weak and the atomic mass small, so that the zero-point energy becomes almost comparable with the potential energy. The rms deviation of an atom from its lattice site is then no longer small with respect to the nearest-neighbor distance and the standard harmonic approximation becomes inadequate for a proper treatment of the crystals. Quantum crystals have been extensively studied in the last ten years and comprehensive

recent reviews may be found in the works of Brandow[16] and Guyer.[17] These studies can be broadly divided into two categories: One is concentrated on the long-range correlations associated with the phonons, while the other deals principally with the short-range correlations arising from the hard-core of the two-body interaction. The latter aspect is usually handled by the *variational* approach adopted, amongst others, by Nosanow,[18] Hansen and Levesque,[19] Massey and Woo[20] and the *t-matrix* approach followed by Iwamoto and Namaizawa,[21] Guyer and Zane,[22] and Sarkissian,[23] Horner,[24] and Ebner and Sung.[25]

The variational approach, in which the trial wave function is written as a product of a single-particle wave functions (taken to be Gaussians centered at lattice sites) and a short-range correlation functions, is based on an approximate expression for the expectation value of the energy which is obtained by performing a truncated cluster expansion in the manner of van Kampen. Most of the theoretical work on the ground-state energy of solid helium has been done using the variational approach. Hansen and Levesque[19] performed a Monte Carlo calculation and obtained the best solidification pressure. The merit of this calculation is that the energy expectation value is based on a cluster development that includes short-range correlations between all particles in successive orders in the expansion; the calculation, however, uses a rather restrictive form of the correlation function which turns out to be considerably more spread out than any of the other published forms.

We have adapted the t-matrix approach to the many-body problem. Even though any two-body theory should be capable of handling the full complexity of the nucleon-nucleon (NN) potential, the presently available formulas in the variational framework[18] are not, as such, suitable to handle the NN problem since they were originally developed for spherically symmetric potentials, like the one acting among two helium atoms.

A detailed t-matrix calculation of solid ^{3}He has been described by Guyer and Zane[22] who used an equation of motion for two particles in the average field produced by the remaining particles similar to the Bethe-Goldstone equation. Also, Horner[24] has reported a Brueckner-type formalism where short-range correlations are included to derive a Bethe-Goldstone type of equation. These calculations, which have yielded ground-state energies in reasonable agreement with the experimental results, were preceded by the work of Iwamoto and Namaizawa[21] who introduced on intuitive grounds an equation of motion very similar to that derived by Guyer and Zane[22] and Sarkissian.[23]

However, in adapting the t-matrix scheme, we have avoided a number of approximations usually introduced in the context of ^{3}He in order to bring out a full dependence of the wave function on spin and angular momentum and made the full use of energetically favorable spin arrangements in conventional lattice structures.

We consider a system of N baryons described by the Hamiltonian

$$H=-\frac{\hbar^2}{2m}\sum_i \nabla_i^2+\sum_{i<j} V_{ij}\,. \tag{1}$$

Here the Slater determinant for the unperturbed system is built up by single-particle wave functions of Gaussian form

$$\varphi(\vec{r}_i)=\frac{\alpha^{3/2}}{\pi^{3/4}}\exp(-\tfrac{1}{2}\alpha^2|\vec{r}_i-\vec{R}_i|^2)\,, \tag{2}$$

where R_i is the ith lattice site, around which the particle is performing an oscillatory motion under the influence of the remaining $(N-1)$ particles. Such an unperturbed wave function, which is strongly localized at the lattice site, is supposed to exhibit the essential features of the actual system. In translationally invariant systems, the unperturbed wave function is usually taken to be a plane wave. Brueckner theory is a low-density expansion, and as such there is no *a priori* reason why it should work for dense systems like solid helium or baryonic lattices. However, the theory has produced remarkably good results for solid helium and hydrogen.[24-26] This could largely be due to the use of Gaussian wave functions since they already contain correlations and, moreover, to the fact that the contributions from three-body correlations are probably much less important in crystals than in translationally invariant systems like liquid helium or neutron liquid, as evidenced from the small value of the wound integral, $\kappa \leq 0.3$.

The thrust of this computation is to find out whether a system of N strongly interacting baryons will minimize the energy by localizing the constituents in a lattice structure rather than in a liquid state under the conditions of density and pressure of interest in the interior of neutron stars (typically, $\rho \simeq 10^{15}$ g/cm^3, $P \simeq 10^{35}$ dynes/cm^2).

The Hamiltonian of the system may be formally separated into $H=H_0+H_1$, where

$$H_0=\sum_i T_i+\tfrac{1}{2}\sum_{ij} W_{ij}\,,$$

$$H_1=\tfrac{1}{2}\sum_{ij}(V_{ij}-W_{ij})\,,$$

The Hamiltonian H_0 is supposed to be exactly solvable leading to localized orbitals of Gaussian form with unknown spread α^{-1}. The eigenfunctions

of H_0 are in turn used to perturb H_1. The Rayleigh-Schrödinger perturbation expansion of the energy shift gives rise to the following expression (cf. Guyer and Zane[22] for details)

$$E = \tfrac{3}{4}N\hbar\omega + \tfrac{1}{2}\sum_{ij}\frac{\int \psi_{ij} V_{ij} \varphi_{ij}\, d^3r_i\, d^3r_j}{\int \psi_{ij}\varphi_{ij}\, d^3r_i\, d^3r_j} \tag{3}$$

in which φ_{ij} is the two-body uncorrelated wave-function taken to be the product $\varphi(i)\varphi(j)$, whereas ψ_{ij} is the correlated two-body wave function to be determined by solving the Bethe-Goldstone equation

$$[T(i)+T(j)+U(i)+U(j)+V_{ij}]\psi_{ij} = \epsilon_{ij}\psi_{ij}\,. \tag{4}$$

Here $T(i)$ and $T(j)$ are respectively the kinetic energies of particles i and j, $U(i)$ and $U(j)$ the corresponding self-consistent one-body potentials and V_{ij} is the two-body interaction potential.

Let us write Eq. (4) by separating center-of-mass and relative coordinates. Thus, using Eq. (2), we have

$$\begin{aligned}\varphi_{ij} &= \varphi(i)\varphi(j)\\ &= \frac{\alpha^{3/2}}{\pi^{3/4}}\exp[-\tfrac{1}{2}\alpha^2(\vec{r}_i-\vec{R}_i)^2]\\ &\quad\times\frac{\alpha^{3/2}}{\pi^{3/4}}\exp[-\tfrac{1}{2}\alpha^2(\vec{r}_j-\vec{R}_j)^2]\,.\end{aligned} \tag{5}$$

Introducing the notation

$$\vec{\Delta} = \vec{R}_i - \vec{R}_j,\quad \vec{\delta} = \frac{m_i\vec{R}_i + m_j\vec{R}_j}{m_i+m_j},\quad \vec{r} = \vec{r}_i - \vec{r}_j\,,$$

$$\vec{R} = \frac{m_i\vec{r}_i + m_j\vec{r}_j}{m_i+m_j},\quad \mu = \frac{m_i m_j}{m_i+m_j}\,, \tag{6}$$

$$\alpha^2 = \frac{2\mu}{\hbar}\omega\,,$$

we can write

$$\varphi_{ij} = \Phi(\vec{R})\varphi(\vec{r})\,, \tag{7}$$

where

$$\begin{aligned}\Phi(\vec{R}) &= (\tfrac{1}{2}\pi)^{-3/4}\alpha^{3/2}\exp[-\alpha^2(\vec{R}-\vec{\delta})^2]\,,\\ \varphi(\vec{r}) &= (2\pi)^{-3/4}\alpha^{3/2}\exp[-\tfrac{1}{4}\alpha^2(\vec{r}-\vec{\Delta})^2]\,,\end{aligned} \tag{8}$$

with

$$\begin{aligned}&\int d^3R\,\Phi^2(\vec{R}) = 1,\\ &\int d^3r\,\varphi^2(\vec{r}) = 1\,.\end{aligned} \tag{9}$$

The Hamiltonian of Eq. (4) may be written as

$$\mathcal{H} = \mathcal{H}(\vec{R}) + \mathcal{H}(\vec{r}) \tag{10}$$

in which

$$\mathcal{H}(\vec{R}) = -\frac{\hbar^2}{8\mu}\nabla_R{}^2 + \tfrac{1}{4}\mu\omega^2[(\vec{R}-\vec{R}_i)^2 + (\vec{R}-\vec{R}_j)^2]\,, \tag{11}$$

$$\mathcal{H}(\vec{r}) = -\frac{\hbar^2}{2\mu}\nabla_r{}^2 + \tfrac{1}{2}\mu\omega^2 r^2 - \mu\omega^2\vec{r}\cdot\vec{\Delta} + 2U(0) + V(\vec{r}), \tag{12}$$

and $U(i) \equiv U(\vec{r}_i - \vec{R}_i)$ has been assumed to be of the form

$$U(0) + \tfrac{1}{2}m\omega^2(\vec{r}_i - \vec{R}_i)^2\,. \tag{13}$$

The determination of $U(0)$ and ω self-consistently will be discussed in Sec. IV. The wave function ψ_{ij} can then be written as

$$\psi_{ij} = \psi(\vec{R})\psi(\vec{r})\,, \tag{14}$$

where

$$\psi(\vec{R}) = \alpha^{3/2}(\tfrac{1}{2}\pi)^{-3/4}e^{-\alpha^2(\vec{R}-\vec{\delta})^2} \tag{15}$$

satisfies the equation

$$\mathcal{H}(\vec{R})\psi(\vec{R}) = (\tfrac{3}{2}\hbar\omega + \tfrac{1}{2}\mu\omega^2\Delta^2)\psi(\vec{R})\,. \tag{16}$$

The equation of motion (4) can finally be written as

$$\left[-\frac{\hbar^2}{2\mu}\nabla_r{}^2 + \tfrac{1}{2}\mu\omega^2(\vec{r}-\vec{\Delta})^2 + V(\vec{r})\right]\psi = [\epsilon - \tfrac{3}{2}\hbar\omega - 2U(0)]\psi\,. \tag{17}$$

The wave function ψ in its full generality must be taken to depend upon M_S, the projection of the total spin S. The general wave function is then written to include the spin wave functions $\chi_s^{M_S}$ (cf. Bethe, Brandow, and Petschek[27]):

$$\psi \equiv \psi^{SM_S}(\vec{r}) = \sum_{lJ} i^l[4\pi(2l+1)]^{1/2}(l0SM_S\,|\,JM)\times\psi_{lJ}^{M_S}(r)\mathcal{Y}_{lJ}^{M_S}(\Omega) \tag{18}$$

in obvious notation.

In our formalism the energy is strongly dependent upon the spin arrangement and we have to consider three distinct possibilities:

(A) $S=0$, $M_S=0$:

$$\psi^{00} = \sum_{l=0}^{\infty} i^l[4\pi(2l+1)]^{1/2}\psi_{ll}^{00}(r)\mathcal{Y}_{ll}^{0}(\Omega)\,,$$

(B) $S=1$, $M_S=0$:

$$\psi^{10} = \sum_{l=0}^{\infty}\sum_{J} i^l[4\pi(2l+1)]^{1/2}(l010\,|\,J0)\times\psi_{lJ}^{10}(r)\mathcal{Y}_{lJ}^{0}(\Omega), \tag{19}$$

(C) $S=1$, $M_S=1$:

$$\psi^{11}=\sum_{l=0}^{\infty}\sum_{J} i^l[4\pi(2l+1)]^{1/2}(l011|J1) \times \psi_{lJ}^{11}(r)\mathcal{Y}_{lJ}^{1}(\Omega).$$

The introduction of i^l in the expansion of the wave function is only formal; it has been introduced to be consistent with the expansion of the unperturbed wave function $\varphi(\vec{r})$ [Eq. (8)] which contains in the exponent a term of the form $\vec{r}\cdot\vec{\Delta}$. The angular part of $\varphi(\vec{r})$ when expanded gives rise to

$$\chi_s^{M_S} e^{\alpha^2\vec{r}\cdot\vec{\Delta}/2}=\sum_{l=0}^{\infty}\sum_{J} i^l[4\pi(2l+1)]^{1/2}(l0SM_S|JM) \times j_l(-\tfrac{1}{2}i\alpha^2 r\Delta)\mathcal{Y}_{lJ}^{M_S}(\Omega), \quad (20)$$

where $j_l(ix)$ is a Bessel function of imaginary argument. After inserting the three wave functions (A), (B), (C), into Eq. (17), we get three sets of coupled differential equations. The coupling of various waves is due to the term $\vec{r}\cdot\vec{\Delta}=r\Delta\cos\theta$ which much like the Stark effect couples odd and even waves.

We have included in our computation partial waves up to $l=6$. This gives rise to three sets of equations containing, respectively, 7, 13, 18 coupled second-order differential equations for cases (A), (B), (C). The solution of these coupled equations in order to yield the lowest eigenvalue (else nodeless wave function) is a formidable task. We have resorted to the power method used in numerical analysis for obtaining the lowest eigenvalue and it is described in detail in the Appendix.

If we now introduce the notation

$$r\psi_{lJ}^{SM_S}=\begin{cases} F_l, & S=0,\ M_S=0 \\ G_{lJ}, & S=1,\ M_S=0 \\ H_{lJ}, & S=1,\ M_S=1 \end{cases} \quad (21)$$

the three sets of equations can be cast in the following form:

(A) $S=0$, $M_S=0$,

$$F_l''+(E-U_{lJ})F_l + \frac{(-1)^{l+1}}{(2l+1)}\frac{a^4 xd}{2}[lF_{l-1}-(l+1)F_{l+1}]=0,$$

(B) $S=1$, $M_S=0$,

$$G_{lJ}''+(E-U_{lJ})G_{lJ} + \frac{(-1)^{l+1}}{(2l+1)}\frac{a^4 xd}{2}\Big[l\sum_{J'}(l+1010|J'0)^2 G_{l+1,J'} -(l+1)\sum_{J''}(l-1010|J''0)^2 G_{l-1,J''}\Big]=0, \quad (22)$$

(C) $S=1$, $M_S=1$,

$$H_{lJ}''+(E-U_{lJ})H_{lJ} + \frac{(-1)^{l+1}}{(2l+1)}\frac{a^4 xd}{2}\Big[l\sum_{J'}(l+1011|J'1)^2 H_{l+1,J'} -(l+1)\sum_{J''}(l-1011|J''1)^2 H_{l-1,J''}\Big]=0.$$

Here $l=0,1,\ldots,6$ and J takes the values compatible with $|l-1|\le J\le l+1$ and likewise the sums over J' and J'' follow the rule:

$$l\le J'\le l+2, \quad |l-2|\le J''\le l.$$

The rest of the notation is as follows:

$$a=\alpha r_0,\quad x=r/r_0,$$
$$d=\frac{\Delta}{r_0},\quad \rho=\frac{\gamma m}{r_0^3},$$
$$U_{lJ}=\tfrac{1}{4}a^4x^2+\frac{2\mu r_0^2}{\hbar^2}V_{lJ}+\frac{l(l+1)}{x^2},$$
$$E=\frac{2\mu r_0^2}{\hbar^2}\left(\epsilon-\tfrac{3}{2}\hbar\omega-\frac{\hbar^2}{8\mu}\alpha^4\Delta^2-2U_0\right). \quad (23)$$

The matter density ρ is so defined that there are four particles per unit cell for an fcc lattice ($\gamma=4$) and two particles for a bcc lattice ($\gamma=2$). Once the wave functions are known for each spin and angular momentum component, for a given frequency ω, the energy per particle can be readily computed.

In this section we have discussed the equation of motion of two particles, each of them moving in a one-body potential centered around different lattice sites and, in addition, interacting through a two-body potential. We shall now derive the expressions for energy per particle up to second order for various pairs of baryons, and in particular develop the detailed formulas for nucleon-nucleon interactions up to $l\le 6$, in the following section.

III. ENERGY EXPRESSIONS

The general expression for energy per particle can be written as [see Eq. (3)]

$$E/N=\tfrac{3}{4}\hbar\omega+\tfrac{1}{2}\sum_k n_k\epsilon_k. \quad (24)$$

The first and second term are not the expectation value of the true kinetic and potential energy in the exact ground state due to the fact that we use a model theory. We shall, however, refer to them simply as kinetic and potential energy with the

understanding of the limitation inherent to such terminology. The quantity n_k is the number of particles in the kth shell and ϵ_k the energy for that shell. The explicit expression for ϵ_k of course depends on the spin configuration under consideration and in what follows we shall derive the formulas for various baryon-baryon interactions and spin configurations.

Let us write the energy expression for the interaction of two particles i, j with a given spin and isotopic-spin projection M_S and T_3 as follows:

$$\epsilon(ij) = \sum_{ST} (\tfrac{1}{2} m_i \tfrac{1}{2} m_j | SM_S)^2 (t_i \tau_i t_j \tau_j | TT_3)^2 \times E(S, M_S, T), \tag{25}$$

where m_i, m_j can take values $\pm\frac{1}{2}$; the values assumed by t_i, t_j and their respective projections τ_i, τ_j depend on the specific pair of baryons under consideration. In general

$$E(S, M_S, T) = \frac{\int \psi^{SM_S}(\vec{r}) V(\vec{r}) \varphi^{SM_S}(\vec{r}) d\vec{r}}{\int \psi^{SM_S}(\vec{r}) \varphi^{SM_S}(\vec{r}) d\vec{r}} . \tag{26}$$

Each $\psi^{SM_S}(\vec{r})$ is the solution of the appropriate set of Eq. (22) and $V(\vec{r})$ is the two-body interaction potential between the particles in question.

After calculating the Clebsch-Gordan coefficients applicable to various particle pairs we derive the following energy expressions:

$$\begin{aligned}
\epsilon_1 &= \epsilon(n_\uparrow n_\uparrow) \\
&= \epsilon(p_\uparrow p_\uparrow) \\
&= E(S=1, M_S=1, T=1), \\
\epsilon_2 &= \epsilon(n_\uparrow n_\downarrow) \\
&= \epsilon(p_\uparrow p_\downarrow) \\
&= \tfrac{1}{2}[E(S=0, M_S=0, T=1) + E(S=1, M_S=0, T=1)], \\
\epsilon_3 &= \epsilon(n_\uparrow p_\uparrow) \\
&= \tfrac{1}{2}[E(S=1, M_S=1, T=0) + E(S=1, M_S=1, T=1)], \\
\epsilon_4 &= \epsilon(n_\uparrow p_\downarrow) \\
&= \tfrac{1}{4}[E(S=0, M_S=0, T=0) + E(S=0, M_S=0, T=1) \\
&\quad + E(S=1, M_S=0, T=0) + E(S=1, M_S=0, T=1)], \\
\epsilon_5 &= \epsilon(\Sigma^-_\uparrow n_\uparrow) \\
&= \epsilon(\Sigma^+_\uparrow p_\uparrow) = E(S=1, M_S=1, T=\tfrac{3}{2}), \\
\epsilon_6 &= \epsilon(\Sigma^-_\uparrow n_\downarrow) \\
&= \epsilon(\Sigma^+_\uparrow p_\downarrow) \\
&= \tfrac{1}{2}[E(S=0, M_S=0, T=\tfrac{3}{2}) + E(S=1, M_S=0, T=\tfrac{3}{2})], \\
\epsilon_7 &= \epsilon(\Sigma^+_\uparrow n_\uparrow) \\
&= \epsilon(\Sigma^-_\uparrow p_\uparrow) \\
&= \tfrac{1}{3}[2E(S=1, M_S=1, T=\tfrac{1}{2}) + E(S=1, M_S=1, T=\tfrac{3}{2})], \\
\epsilon_8 &= \epsilon(\Sigma^+_\uparrow n_\downarrow) \\
&= \epsilon(\Sigma^-_\uparrow p_\downarrow) \\
&= \tfrac{1}{6}[2E(S=0, M_S=0, T=\tfrac{1}{2}) + E(S=0, M_S=0, T=\tfrac{3}{2}) \\
&\quad + 2E(S=1, M_S=0, T=\tfrac{1}{2}) + E(S=1, M_S=0, T=\tfrac{3}{2})], \\
\epsilon_9 &= \epsilon(\Sigma^0_\uparrow n_\uparrow) \\
&= \epsilon(\Sigma^0_\uparrow p_\uparrow) \\
&= \tfrac{1}{3}[2E(S=1, M_S=1, T=\tfrac{3}{2}) + E(S=1, M_S=1, T=\tfrac{1}{2})], \\
\epsilon_{10} &= \epsilon(\Sigma^0_\uparrow n_\downarrow) \\
&= \epsilon(\Sigma^0_\uparrow p_\downarrow) \\
&= \tfrac{1}{6}[2E(S=0, M_S=0, T=\tfrac{3}{2}) + E(S=0, M_S=0, T=\tfrac{1}{2}) \\
&\quad + 2E(S=1, M_S=0, T=\tfrac{3}{2}) + E(S=1, M_S=0, T=\tfrac{1}{2})], \\
\epsilon_{11} &= \epsilon(\Lambda_\uparrow n_\uparrow) \\
&= \epsilon(\Lambda_\uparrow p_\uparrow) \\
&= E(S=1, M_S=1, T=\tfrac{1}{2}), \\
\epsilon_{12} &= \epsilon(\Lambda_\uparrow n_\downarrow) \\
&= \epsilon(\Lambda_\uparrow p_\downarrow) \\
&= \tfrac{1}{2}[E(S=0, M_S=0, T=\tfrac{1}{2}) + E(S=1, M_S=0, T=\tfrac{1}{2})], \\
\epsilon_{13} &= \epsilon(\Lambda_\uparrow \Lambda_\downarrow) \\
&= E(S=1, M_S=1, T=0), \\
\epsilon_{14} &= \epsilon(\Lambda_\uparrow \Lambda_\downarrow) \\
&= \tfrac{1}{2}[E(S=0, M_S=0, T=0) + E(S=1, M_S=0, T=0)], \\
\epsilon_{15} &= \epsilon(\Sigma^0_\uparrow \Sigma^0_\uparrow) \\
&= \tfrac{1}{3}[2E(S=1, M_S=1, T=2) + E(S=1, M_S=1, T=0)], \\
\epsilon_{16} &= \epsilon(\Sigma^0_\uparrow \Sigma^0_\downarrow) \\
&= \tfrac{1}{6}[2E(S=0, M_S=0, T=2) + E(S=0, M_S=0, T=0) \\
&\quad + 2E(S=1, M_S=0, T=2) + E(S=1, M_S=0, T=0)], \\
\epsilon_{17} &= \epsilon(\Sigma^+_\uparrow \Sigma^+_\uparrow) \\
&= \epsilon(\Sigma^-_\uparrow \Sigma^-_\uparrow) \\
&= E(S=1, M_S=1, T=2), \\
\epsilon_{18} &= \epsilon(\Sigma^+_\uparrow \Sigma^+_\downarrow) \\
&= \epsilon(\Sigma^-_\uparrow \Sigma^-_\downarrow) \\
&= \tfrac{1}{2}[E(S=0, M_S=0, T=2) + E(S=1, M_S=0, T=2)], \\
\epsilon_{19} &= \epsilon(\Sigma^+_\uparrow \Sigma^0_\uparrow) \\
&= \epsilon(\Sigma^-_\uparrow \Sigma^0_\uparrow) \\
&= \tfrac{1}{2}[E(S=1, M_S=1, T=1) + E(S=1, M_S=1, T=2)],
\end{aligned} \tag{27}$$

$$\epsilon_{20} = \epsilon(\Sigma^{\dagger}_{\uparrow}\Sigma^{0}_{\uparrow})$$
$$= \epsilon(\Sigma^{-}_{\uparrow}\Sigma^{0}_{\uparrow})$$
$$= \tfrac{1}{4}[E(S=0,M_S=0,T=1)+E(S=0,M_S=0,T=2)$$
$$+E(S=1,M_S=0,T=1)+E(S=1,M_S=0,T=2)],$$

$$\epsilon_{21} = \epsilon(\Sigma^{\dagger}_{\uparrow}\Sigma^{-}_{\uparrow})$$
$$= \tfrac{1}{6}[3E(S=1,M_S=1,T=1)+2E(S=1,M_S=1,T=0)$$
$$+E(S=1,M_S=1,T=2)],$$

$$\epsilon_{22} = \epsilon(\Sigma^{\dagger}_{\uparrow}\Sigma^{-}_{\downarrow})$$
$$= \tfrac{1}{12}[3E(S=0,M_S=0,T=1)+2E(S=0,M_S=0,T=0)$$
$$+E(S=0,M_S=0,T=2)+3E(S=1,M_S=0,T=1)$$
$$+2E(S=1,M_S=0,T=0)+E(S=1,M_S=0,T=2)],$$

$$\epsilon_{23} = \epsilon(\Sigma^{0}_{\uparrow}\Lambda_{\uparrow})$$
$$= \epsilon(\Sigma^{\dagger}_{\uparrow}\Lambda_{\downarrow})$$
$$= \epsilon(\Sigma^{-}_{\uparrow}\Lambda_{\uparrow})$$
$$= E(S=1,M_S=1,T=1),$$

$$\epsilon_{24} = \epsilon(\Sigma^{0}_{\uparrow}\Lambda_{\downarrow})$$
$$= \epsilon(\Sigma^{\dagger}_{\uparrow}\Lambda_{\downarrow})$$
$$= \epsilon(\Sigma^{-}_{\uparrow}\Lambda_{\downarrow})$$
$$= \tfrac{1}{2}[E(S=0,M_S=0,T=1)+E(S=1,M_S=0,T=1)].$$

Using Eqs. (8), (18), (20), and (21), the four possibilities for the n-p system give

$$\epsilon_1 = \epsilon(n_{\uparrow}n_{\uparrow})$$
$$= N_{11}^{-1}\int\{3[H_{11}V(^3P_1)+H_{12}V(^3P_2)]j_1+[2H_{32}V(^3F_2)+7H_{33}V(^3F_3)+5H_{34}V(^3F_4)]j_3+\cdots\}a(x)dx,$$

$$\epsilon_2 = \epsilon(n_{\uparrow}n_{\downarrow})$$
$$= \frac{1}{2}\Big(N_{21}^{-1}\int[F_0V(^1S_0)j_0+5F_2V(^1D_2)j_2+9F_4V(^1G_4)j_4+\cdots]a(x)dx$$
$$+N_{22}^{-1}\int\{[2G_{12}V(^3P_2)+G_{10}V(^3P_0)]j_1+[3G_{32}V(^3F_2)+4G_{34}V(^3F_4)]j_3+\cdots\}a(x)dx\Big),$$

$$\epsilon_3 = \epsilon(n_{\uparrow}p_{\uparrow})$$
$$= \tfrac{1}{2}\Big(N_{31}^{-1}\int\{3[H_{11}V(^3P_1)+H_{12}V(^3P_2)]j_1+[2H_{32}V(^3F_2)+7H_{33}V(^3F_3)+5H_{34}V(^3F_4)]j_3+\cdots\}a(x)dx$$
$$+N_{32}^{-1}\int\{H_{01}V(^3S_1)j_0+\tfrac{5}{2}[H_{22}V(^3D_2)+\tfrac{1}{5}H_{21}V(^3D_1)]j_2+\cdots\}a(x)dx\Big),$$

$$\epsilon_4 = \epsilon(n_{\uparrow}p_{\downarrow})$$
$$= \tfrac{1}{4}\Big(N_{41}^{-1}\int[3F_1V(^1P_1)j_1+7F_3V(^1F_3)j_3+\cdots]a(x)dx+N_{42}^{-1}\int[F_0V(^1S_0)j_0+5F_2V(^1D_2)j_2+9F_4V(^1G_4)j_4]a(x)dx$$
$$+N_{43}^{-1}\int\{[2G_{12}V(^3P_2)+G_{10}V(^3P_0)]j_1+[3G_{32}V(^3F_2)+4G_{34}V(^3F_4)]j_3+\cdots\}a(x)dx$$
$$+N_{44}^{-1}\int\{[G_{01}V(^3S_1)j_0+2G_{21}V(^3D_1)j_2+\cdots]\}a(x)dx\Big), \tag{28}$$

where $N_{\alpha\beta}^{-1}$ is the same as the numerator with $V=1$. The various quantities are defined as

$$y=\tfrac{1}{2}a^2xd,\quad a(x)=xe^{-a^2x^2/4},$$
$$j_0=\frac{\sinh y}{y},$$
$$j_1=\frac{\cosh y}{y}-\frac{\sinh y}{y^2}, \tag{29}$$
$$j_2=\frac{3\cosh y}{y^2}-\left(\frac{1}{y}+\frac{3}{y^3}\right)\sinh y.$$

In general

$$j_n(x)=(-x)^n\left(\frac{1}{x}\frac{d}{dx}\right)^n\left(\frac{\sin x}{x}\right).$$

IV. DETERMINATION OF THE FREQUENCY OF OSCILLATION

One of the important parameters in the present formulation is the spread α^{-1} of the single-particle wave function, which is related to ω of Eq. (24) by the relation,

$$\alpha^2 = m\omega/\hbar \ . \tag{30}$$

The determination of α is a difficult task and we shall describe the way in which we have proceeded:

When the quantum crystal problem is treated within the variational framework the energy is usually varied with respect to α until a minimum is found. However, in the t-matrix computations of solid ^{3}He so far published, one finds that both methods have been employed: The minimization of E/N vs α and the determination of α self-consistently. The latter may be carried out as follows. In the framework of the t matrix one defines the one-body potential $U(i)$ as

$$\varphi(i)U(i)\varphi(i) = \sum_{j=1}^{N} \frac{\int \varphi(i)\varphi(j)V_{ij}\psi_{ij}d^3r_j}{\int\int \varphi(i)\varphi(j)\psi_{ij}d^3r_i\, d^3r_j}, \tag{31}$$

where ψ is taken to be antisymmetrized, i.e., only the waves allowed by the Pauli principle are employed. (See discussion in Sec. X.)

Using the previous definition of $\varphi(i)$ given in Eq. (2), the numerator of Eq. (31) becomes

$$\frac{\alpha^{9/2}}{(2\pi)^{3/4}(\frac{1}{2}\pi)^{3/2}} \int \exp[-\tfrac{1}{2}\alpha^2(2\vec{\rho}_i + \vec{r} - \vec{\Delta})^2] \times \exp[-\tfrac{1}{4}\alpha^2(\vec{r} - \vec{\Delta})^2]\psi(\vec{r})V(\vec{r})d^3r, \tag{32}$$

where $\vec{\rho}_i = \vec{r}_i - \vec{R}_i$. Similarly, the denominator can be rewritten as

$$\frac{\alpha^{3/2}}{(2\pi)^{3/4}} \int \exp[-\tfrac{1}{4}\alpha^2(\vec{r} - \vec{\Delta})^2]\psi(\vec{r})d^3r \ . \tag{33}$$

Since the one-body potential is considered to be of the form $U(0) + \frac{1}{2}m\omega^2(\vec{r}_i - \vec{R}_i)^2$ we compute $U(i)$ at the lattice site, i.e., we evaluate Eq. (31) at $\vec{r}_i = \vec{R}_i$, thus obtaining after some algebra the exact expression:

$$U(0) = 2\sqrt{2}\sum_k n_k \frac{\int \exp[-\frac{3}{4}\alpha^2(\vec{r} - \vec{\Delta})^2]\, V(\vec{r})\psi(\vec{r})d^3r}{\int \exp[-\frac{1}{4}\alpha^2(\vec{r} - \vec{\Delta})^2]\psi(\vec{r})d^3r} \tag{34}$$

Let us now obtain a second expression for $U(0)$ by inserting Eq. (31) into Eq. (3). Using Eq. (13), the energy per particle may then be written as:

$$\frac{E}{N} = \tfrac{3}{4}\frac{\hbar^2}{m}\alpha^2 + \tfrac{1}{2}U(0) + \tfrac{1}{2}\,\frac{3}{4}\,\frac{\hbar^2}{m}\alpha^2$$

$$= \frac{9}{8}\frac{\hbar^2}{m}\alpha^2 + \tfrac{1}{2}U(0) \ . \tag{35}$$

Since by definition

$$\frac{E}{N} = \frac{3}{4}\frac{\hbar^2}{m}\alpha^2 + \tfrac{1}{2}\sum_k n_k\epsilon_k \ ,$$

we can recombine the foregoing equations to get $U(0)$, now called $U^D(0)$ in the form

$$U^D(0) = \sum_k n_k\epsilon_k - \frac{3}{4}\frac{\hbar^2}{m}\alpha^2$$

$$\equiv 2(\text{Pot. En.}) - (\text{Kin. En.}) \ . \tag{36}$$

Our computation now proceeds as follows: Given an arbitrary ω we solve Eq. (22), compute ψ, substitute it in Eq. (34) and evaluate $U(0)$. Once the ψ's are known, they are also used to compute ϵ_k with the help of Eqs. (24)–(27). From Eq. (36), $U^D(0)$ is then determined. The procedure is repeated for several ω's, and a plot is made of $U(0)$ and $U^D(0)$ vs ω (or α^2) with the intersection of the two curves determining the self-consistent value of ω. This value is then employed to recompute ψ and finally the energy using Eq. (24). Now an important question is: How does the α so obtained compare to the one given by the relation $\partial(E/N)/\partial\alpha = 0$?

Unfortunately it has not been easy to answer this question from the published literature. As far as the authors were able to reconstruct either method was used exclusively and no direct comparison is therefore possible.

In order to gain a better understanding of the problem, we performed two calculations, which though not directly related to the present problem, are nevertheless rather instructive. After employing the present technique for handling the angular momentum dependence of the B-G equation for solid ^{3}He, the resulting ψ was used to compute $(E/N)_v$ and $(E/N)_t$, the variational and t-matrix energies. The function $(E/N)_v$ was found to have a very clear minimum with respect to α at $\alpha = \alpha_v$. The value of α_v was however higher than the value of α determined self-consistently. The values for the energy were nevertheless almost identical. Second, we performed a neutron-solid computation assuming the same potential for all the angular momentum waves. In particular, we took

$$V(r) = 6484.2\frac{e^{-7x}}{x}, \qquad x = 0.7r,$$

which is the repulsive part of Reid's $^1S_0$ potential, a potential suggested to us by Bethe.

The results were as follows:

(1) The ψ's obtained from the B-G equation were used in the variational form for E/N and the energy was then minimized with respect to α. A clear minimum existed at α_v. The same ψ was also substituted into the t-matrix form of E/N and α was determined both by minimizing E/N (again a minimum existed) and by using the self-consistency equations. The latter two α's were

extremely close but both smaller than α_v.

(2) The energies $(E/N)_t$ and $(E/N)_v$ were almost identical. In a sense this fictituous problem greatly resembles the ^{3}He case, since only a state-independent potential is employed and the behavior of $V(r)$ for small r is the same for all the angular momentum waves.

(3) When one goes from the $V(r)$ just described to a realistic potential, for instance the one given by Reid, then $(E/N)_t$ has a very shallow minimum with respect to α, if a minimum exists at all. We have not tried to employ the B-G ψ's in $(E/N)_v$, as done previously, since the presently available equations for $(E/N)_v$ are not suited to state-dependent f's. We therefore determined α through the full self-consistent method described before. At this point the suspicion could arise that the behavior of Reid's potential near the origin, which is rather different for different waves, is responsible for the disappearance of a well-defined minimum. Reid's potential is presently being studied by Bethe and Johnson with a view toward constructing a new potential having the same core behavior for all angular momentum states. It is too early to decide as to whether this new potential will give substantially different results, but it is surely safe to expect that the behavior near the origin of $V(r)$ has a major influence on the E/N vs α behavior.

V. SPIN CONFIGURATIONS IN A LATTICE

The nuclear forces are known to be highly spin- and angular-momentum-dependent. One of the main motivations of our computation was to attempt a number of spin arrangements by localizing the particles in a variety of configurations with a view to minimize the energy. The overriding consideration was to collect as many particles with antiparallel spins in the neighborhood of a given particle so that the singlet $^1S_0$ which is an attractive potential in the range of density under consideration will become operative, thus lowering the energy. Clearly we must aviod a configuration with too many particles with parallel spins in the first few neighboring shells. The reason for this may be attributed to the frequent appearance of the triplet $^3P_1$, a state in which nucleons always repel each other at any distance.

For a given lattice structure we can arrange the baryons in a large number of ways depending upon the spin configuration. In a bcc lattice, for instance, there are two interpenetrating cubes with 16 possible sites and if one is considering a system of an equal number of neutrons and protons, there are eight possible sites for neutrons and eight for protons. Note that we are considering a larger unit cell compared to the conventional concept of a unit cell for a cubic structure. One could start with any site of a cube with, say, a neutron with its spin up, $n_\uparrow$. In the adjacent site on the same cube one can put $n_\downarrow$, $p_\uparrow$, or $p_\downarrow$. In the next site one has a similar kind of degeneracy and the same degeneracy can be thought of for the interpenetrating cube. In general one can envisage the most asymmetrical configuration with respect to the kind of particles and their spins randomly distributed at lattice sites. We tried several of these configurations with an arbitrary degree of randomness to ensure that they are not energetically favorable. It soon became clear that for a given configuration the energetically favorable situation occurs whenever the spins of the particles are symmetrically distributed.

Regarding an fcc lattice made up of neutrons there are the following three symmetrical possibilities for the arrangement of the spins:

(1) In an fcc structure, basically there are four cubes—a simple cube with three other cubes whose corners are at the face-centers of the simple cube. The neutrons can be so distributed that any two neutrons at the adjacent corners of the same simple cube have opposite spins. The same distribution is applied to the other three cubes which are displayed as face-centers in Fig. 1(a). We call this the "mixed spins" configuration.

(2) The spins of the neutrons on the basic cube can be all parallel, say $\uparrow$, and in the three face-centered cubes the spins can be all parallel, with one cube having all spins up ($\uparrow$) and two cubes with all spins down ($\downarrow$), as exhibited in Fig. 1(b). This is our "parallel spins" configuration.

(3) Another possibility is that one can start with the spins of neutrons in a given cube parallel and up ($\uparrow$) and the spins of the three face-centered cubes can be antiparallel and down ($\downarrow$) as shown in Fig. 1(c). Notice that we are considering a larger unit cell compared to the conventional unit cell and as the system is translationally invariant, the symmetry of the spin configurations repeats over the whole crystal.

The spin configurations for the three cases are shown in Fig. 1 for the first four shells. In cases (b) and (c) we see the spin configuration $\epsilon_1(n_\uparrow n_\uparrow)$ repeating in every other shell starting with the second shell and this implies a preponderance of the $^3P_1$ which is purely repulsive. In case (a), however, in the second shell we have $\epsilon_2(n_\uparrow n_\downarrow)$ and this collects attraction from the presence of the singlet $^1S_0$ wave, while $\epsilon_1(n_\uparrow n_\uparrow)$ does not appear till the fourth shell at which distance its repulsive contribution is significantly lower. This is the main reason for favoring the fcc configuration of neutrons with mixed spins, a fact which is indeed

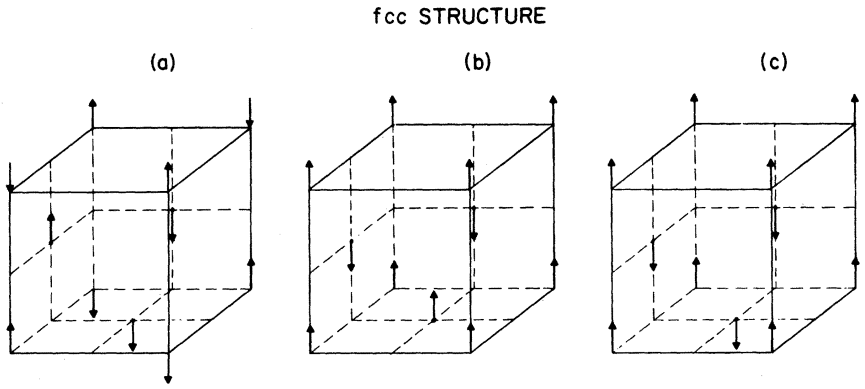

	N_K	ϵ_K	ϵ_K	ϵ_K
①	12	$\frac{1}{2}(\epsilon_1+\epsilon_2)$	$\frac{1}{3}(\epsilon_1+2\epsilon_2)$	$\frac{1}{2}(\epsilon_1+\epsilon_2)$
②	6	ϵ_2	ϵ_1	ϵ_1
③	24	$\frac{1}{2}(\epsilon_1+\epsilon_2)$	$\frac{1}{3}(\epsilon_1+2\epsilon_2)$	$\frac{1}{2}(\epsilon_1+\epsilon_2)$
④	12	ϵ_1	ϵ_1	ϵ_1

$\epsilon_1 = \uparrow\uparrow$ $\epsilon_2 = \downarrow\uparrow$

FIG. 1. Spin configurations for three fcc lattices of neutrons. (a) Mixed spins, where each of the four cubes has neutrons on the adjacent corners with opposite spins, (b) parallel spins, where two out of four cubes have neutrons with their spins parallel and up (↑) and the other two have neutrons with spins parallel and down (↓). Configuration (c) is explained in the text in Sec. V.

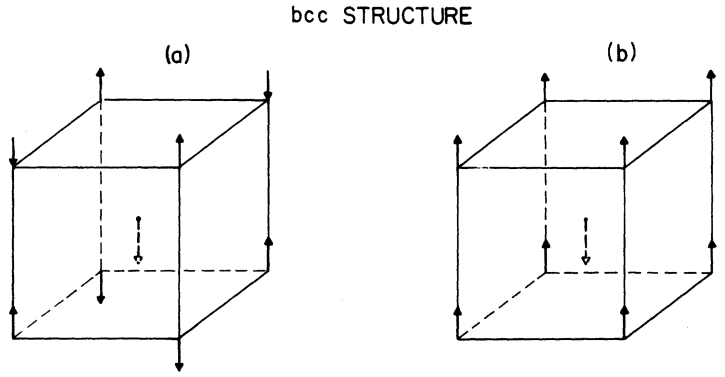

	N_K	ϵ_K	ϵ_K
①	8	$\frac{1}{2}(\epsilon_1+\epsilon_2)$	ϵ_2
②	6	ϵ_2	ϵ_1
③	12	ϵ_1	ϵ_1
④	24	$\frac{1}{2}(\epsilon_1+\epsilon_2)$	ϵ_2

$\epsilon_1 = \uparrow\uparrow$ $\epsilon_2 = \downarrow\uparrow$

FIG. 2. Spin configurations for two bcc lattices of neutrons. (a) Mixed spins, where the two interpenetrating cubes have neutrons on the adjacent corners of the same cube with antiparallel spins, (b) parallel spins, with the neutrons on one cube with spins parallel and (↑) and the interpenetrating cube has neutrons with spins down (↓).

supported by detailed numerical results.

Similarly, for a bcc structure made up of neutrons, the following two possibilities arise:

(1) In a bcc lattice there are two interpenetrating simple cubes. The neutrons can be so distributed that any two neutrons at the adjacent corners of the same simple cube have antiparallel spins. The same symmetry is repeated for the interpenetrating simple cube. This is the bcc mixed-spins configuration displayed in Fig. 2(a).

(2) Another possibility is that the neutrons on the same simple cube can have their spins parallel, say up ↑, while the neutrons on the interpenetrating cube have spins down (↓). We call this the bcc parallel spins case and it is shown in Fig. 2(b).

By and large, the first three shells just about determine the major contribution to the potential energy. It is clear from the spin configurations shown in Fig. 2 that while in the bcc mixed spins case there are ten antiparallel neighbors, there are correspondingly eight antiparallel neighbors in the parallel spins case. In case (b) we have again a preponderance of the spin configuration $\epsilon_1(n_\uparrow n_\uparrow)$ bringing in too much repulsion and consequently case (a) turns out to be energetically more favorable compared to case (b). The detailed computations also bring out the feature that the mixed spins case is to be preferred.

Now, between bcc and fcc mixed spins configurations, the fcc lattice turns out to be energetically favorable since in a fcc structure, in the first three shells, there are 24 antiparallel neighbors while in a bcc there are only ten. Also, at the same density two neutrons are more widely spaced in an fcc than in a bcc lattice and this helps in picking up less repulsion at the high density if the particles are localized in an fcc structure. The hcp structure gives results which are essentially similar to the fcc structure which we have discussed above. We shall exhibit, in what follows, the detailed computations obtained with an fcc lattice of neutrons with mixed spins.

VI. ELASTICITY OF BARYONIC LATTICES

We have hitherto considered the energetics of an hypothetical arrangement of neutrons. In other words, we have assumed the particles to be localized at lattice sites of a specific structure interacting via an assumed nuclear force and then determined the resulting energy per particle. If it should turn out that the energy so obtained is lower than the corresponding energy yielded by assuming a fluid phase, it will be hasty to conclude that the structure represents a solid in an ordinary sense. The question that must be answered is whether such a lattice is mechanically stable. Of course, any lattice has to satisfy the requirement that its energy density must have a stationary value at equilibrium. However, for the structure to be stable, any deformation under shearing stresses must result in an increase of the energy.

We shall follow the notation developed by Born[28] for investigating the mechanical stability of a cube with side 2a which is deformed homogeneously into a parallelepiped whose sides are the vectors $\vec{r}_1, \vec{r}_2, \vec{r}_3$. Consequently the lattice points of the undistorted cube which are described by

$$R_0 = (l_1 a, l_2 a, l_3 a)$$

are then given by the vectors

$$\vec{R}_\delta = l_1\vec{r}_1 + l_2\vec{r}_2 + l_3\vec{r}_3,$$

where the integers l_1, l_2, l_3 assume different sets of values for the bcc, fcc lattices. If we now consider small deformations, the square of the distance from the origin is given by

$$R_\delta^2 = R_0^2 + a^2 \sum_{\alpha\beta} e_{\alpha\beta} l_\alpha l_\beta \equiv R_0^2 + \delta, \tag{37}$$

where $e_{\alpha\beta}$ are the usual strain components of the theory of elasticity:

$$e_{kk} = (r_k^2 - a^2)/a^2, \quad k = 1, 2, 3$$

$$e_{kp} = \vec{r}_k \cdot \vec{r}_p / a^2, \quad k, p = 1, 2, 3.$$

The total potential energy of a deformed lattice $(E/N)_\delta$ wherein the interparticle forces $\Phi(r_{ij})$ are only central, may be written as

$$(E/N)_\delta = \tfrac{1}{2} \sum \Phi\big((R_0^2 + \delta)^{1/2}\big), \tag{38}$$

where the summation symbol is hereafter meant to indicate sum over successive shells.

Since for any well-behaved function $\Phi(r)$, we have

$$\frac{d}{d\delta}\Phi\big((R_0^2+\delta)^{1/2}\big) = \left(\frac{1}{r}\frac{d}{dr}\Phi\right)_{r=(R_0^2+\delta)^{1/2}} \equiv (D\Phi)_{r=(R_0^2+\delta)^{1/2}}$$

we may expand $\Phi(r)$ in a Taylor series as follows:

$$\Phi\big((R^2+\delta)^{1/2}\big) = \Phi(R_0) + \delta(D\Phi)_{R_0} + \tfrac{1}{2}\delta^2(D^2\Phi)_{R_0} + \cdots,$$

and hence rewrite Eq. (38) as

$$\begin{aligned}(E/N)_\delta &= \tfrac{1}{2}\sum(\Phi + \delta D\Phi + \tfrac{1}{2}\delta^2 D^2\Phi + \cdots) \\ &= (E/N)_0 + \tfrac{1}{4}a^2 \sum_{\alpha\beta} e_{\alpha\beta} l_\alpha l_\beta D\Phi \\ &\quad + \frac{a^2}{16}\sum_{\alpha\beta\mu\nu} e_{\alpha\beta} e_{\mu\nu} l_\alpha l_\beta l_\mu l_\nu D^2\Phi + \cdots.\end{aligned} \tag{39}$$

In this expansion the first term on the right-hand side is the energy of the undeformed cube while the second term is zero at equilibrium. We, therefore, have for the deformation energy ΔE

$$\Delta E = \tfrac{1}{2}C_{11}(e_{xx}^2 + e_{yy}^2 + e_{zz}^2) + C_{12}(e_{yy}e_{zz} + e_{zz}e_{xx} + e_{xx}e_{yy}) + \tfrac{1}{2}C_{44}(e_{yz}^2 + e_{zx}^2 + e_{xy}^2) . \quad (40)$$

Here

$$C_{11} = \frac{2a}{\gamma^*}\sum D^2\Phi l_1^4 - P ,$$
$$C_{12} = \frac{2a}{\gamma^*}\sum D^2\Phi l_1^2 l_2^2 , \quad (41)$$
$$C_{44} = \frac{2a}{\gamma^*}\sum D^2\Phi l_1^2 l_2^2 - P ,$$
$$\gamma^* = 4(\text{bcc}), \quad \gamma^* = 2(\text{fcc}), \quad V = \gamma^* a^3 ,$$

where as before the summation extends over successive shells and P is the pressure.

If we now identify R_δ with Δ, the distance from the origin of the various shells, we can compute the first and second derivatives of the potential energy at successive shells and sum over a desired number of shells until a sensible convergence is achieved, and evaluate the elastic constants as a function of the matter density ρ. The above expressions are evidently classical as there is no wave function present in them. The quantum-mechanical expressions may be derived by changing $\Phi(R_{ij})$ into

$$\Phi(R_{ij}) \to \int \varphi(i)\varphi(j)V_{ij}\psi_{ij}\,dr_i\,dr_j .$$

The crystalline structure is deemed stable in the classical sense if $\Delta E > 0$, i.e., if there is a gain in energy while undergoing a small deformation. It is straightforward to show that the quadratic form (40) is positive-definite provided the following considerations are satisfied:

$$\text{(i)}\ \frac{3}{K} \equiv C_{11} + 2C_{12} > 0 \quad (K = \text{compressibility}),$$
$$\text{(ii)}\ C_{44} > 0 , \quad (42)$$
$$\text{(iii)}\ C_{11} - C_{12} > 0 .$$

If condition (i) is violated, the lattice has no cohesion and it is basically unstable. In the event of condition (ii) not being satisfied, there is an absence of elastic resistance to any shearing stresses and the lattice melts. However, if condition (iii) is violated, there may yet be an elastic resistance to shearing stresses, but the material exists in a "gel" form. Physically it is clear that the elastic constant C_{44} represents the shear modulus as it multiplies that part of the deformation energy which is proportional to the nondiagonal terms e_{yz}, e_{zx}, etc. In reality there can be no ambiguity in the concept of melting. If one regards the difference between a liquid and a solid as that the solid offers elastic resistance against shearing stresses while the liquid does not, it would then seem that the positive value of C_{44} is a necessary condition for a crystalline phase to exist.

VII. DISCUSSION

The whole thrust of the calculation is the solution of the three sets of equations, which confronts us with several problems which are discussed below.

Contrary to the uncoupled case, there is no general Sturm-Liouville type of theorem that helps in localizing the lowest eigenvalue. The systems of Eqs. (22) have an infinite set of solutions and the lowest energy eigenvalue has to be searched essentially by a method of trial and error. A detailed description of our numerical method is given in the Appendix. The power method used for this purpose was checked by changing widely the lowest possible eigenvalue and making sure the system indeed converged to the same value, and also by testing it against the $V = 0$ case for which an analytical solution is known. For the $V = 0$ case the numerical value which our method yielded was exact to within one part in 10^3 of the analytical value.

The second problem arises as follows. In Eq. (22) we have l ranging from 0 to infinity. However, for the computation to be manageable, some finite l must be chosen, $l_{\max}$, say, such that the final energy remains unaltered if the contribution of $l_{\max} + 1$ is included. We first included partial waves up to $l \leq 2$. Following a remark by Bethe, we extended the computations up to $l = 4$ and subsequently up to $l = 6$, which for the set (A) $S = 0$, $M_S = 0$ gives rise to seven coupled differential equations. However, since for the triplet states $|l - 1| \leq J \leq l + 1$, the two sets (B) $S = 1$, $M_S = 0$ and (C) $S = 1$, $M_S = 1$ yield, respectively, 13 and 18 coupled differential equation. Even though the energy was found to be sensibly unaltered from say $l = 5$ to $l = 6$, we extended the triplet waves to include $l = 7$ to ascertain that the results were stable. On the other hand, the singlet states for which $l = J$ was extended up to $l = 25$ without too much computational problem. This was also done with hardly any change in the final result. Even though it is impossible for us to establish a mathematical proof of the convergence with respect to the value of l, we however can give the following argument due to Brandow[29] to justify our choice.

The Fourier transform of the single-particle wave function

$$\phi(\vec{r}_i) \propto \exp[-\tfrac{1}{2}\alpha^2(\vec{r}_i - \vec{R}_i)^2]$$

is given by

$$\phi(\vec{\kappa}) \propto \exp(-\kappa^2/2\alpha^2) .$$

The one-body momentum distribution $\phi(\vec{\kappa})^2$ is then proportional to

$$e^{-\kappa^2/\alpha^2}$$

and the root-mean-square of κ comes out to be $(3\alpha^2/2)^{1/2}$.

Now the relative momentum of particles i and j localized in a lattice is

$$\vec{\kappa}_{ij} = \tfrac{1}{2}(\vec{\kappa}_i - \vec{\kappa}_j),$$

and the average gives

$$\langle \kappa_{ij}{}^2 \rangle = \tfrac{1}{4}\langle \kappa_i{}^2 + \kappa_j{}^2 \rangle .$$

The root-mean-square relative $\vec{\kappa}$ is then given by

$$\kappa_{ij} = \left(\frac{1}{2} \times \frac{3\alpha^2}{2}\right)^{1/2}$$

$$= \alpha(\tfrac{3}{4})^{1/2} .$$

The impact-parameter rule consequently yields

$$l \cong \kappa_{ij}\sigma = \alpha\sigma(\tfrac{3}{4})^{1/2} \quad (\sigma\text{: core radius}).$$

Thus to account for the repulsive part of the potential we must include the partial waves up to $l = \alpha\sigma(\frac{3}{4})^{1/2}$, which is of the order of 3 up to a density of 4.4×10^{15} g/cm^3 if we take $\sigma = 1$ (fermi) as the core-radius. The question now arises as to what the value of $l_{\max}$ is to get a fair representation of the maximum of the unperturbed wave function

$$\phi(\vec{r}) \propto e^{-\alpha^2(\vec{r}-\vec{\Delta})^2/4}$$

which occurs in the region where the potential is largely attractive in the range of density of interest. If we take $r = \Delta$ and let θ be the angle between $\vec{r}$ and Δ, then clearly

$$\tfrac{1}{4}\alpha^2(\vec{r} - \vec{\Delta})^2 = \tfrac{1}{2}\alpha^2\Delta^2(1 - \cos\theta),$$

and hence the wave function is reduced by a factor of e when

$$\tfrac{1}{2}\alpha^2\Delta^2(1 - \cos\theta^*) = 1$$

or

$$\cos\theta^* = 1 - \frac{2}{\alpha^2\Delta^2} .$$

The required $l_{\max}$ which is then of the order of π/θ^* is listed in Table I for three densities for the first shell of an fcc lattice of neutrons. The inclusion of partial waves with $l = 6$ is probably adequate for getting a reasonable representation of the correlated wave functions. The problem of convergence is related to the presence of the term $\vec{r}\cdot\vec{\Delta}$ in the equation of motion which couples odd and even waves. A problem of this kind would naturally not arise if one had treated $U(i) + U(j)$ in Eq. (4) not as the sum of two inginite harmonic oscillators, but rather as a clipped harmonic oscillator in the relative coordinate $\vec{r}$. Such a shape would be more physical in that it would allow any of the two particles to be in either well rendering them indistinguishables as they should be. By not so doing one has brought in partial waves which should not be present. In particular, the $S = 0$ state for neutron matter is represented only by $^1S_0$, $^1D_2, \ldots$, i.e., only even-l waves should be present, whereas the coupling term in our formulation brings in unwanted waves like $^1P_1$, etc., i.e., odd-l waves. Analogously, for the triplet state one has to incorporate spurious states like $^3S_1$. The way to deal with such "unwanted" states is not obvious since after all one is paying for the consequences of not having treated the dynamic equation properly. However, it must be stressed that a clipped potential cannot be easily parametrized in a form that renders Eq. (4) mathematically manageable. Recently, a potential of this form has been utilized in the study of single-particle energy levels with reference to fission problems. No extension to a two-body problem is known to the authors. It is our hope that the work done in the two-centered harmonic oscillators in the context of shell-model computations will provide us with some insight into the way to treat such a potential. Lacking any better alternative, we tried several choices for the presence of the undesirable waves.

Choice 1: In the singlet set, $V(^1P_1)$ was taken to be the same as given by Reid, and likewise in the triplet sets, the even waves $V(^3S_1)$ and $V(^3D_J)$ were taken to be those given by Reid. For potentials for higher partial waves in all the states, we chose $V(l>3)_{\text{even}} = V(^1D_2)$ and $V(l \geq 3)_{\text{odd}}$

TABLE I. The values of $l_{\max}$ required to get a fair representation of the maximum of the unperturbed wave function $\phi(\vec{r}) \propto \exp[-\frac{1}{4}\alpha^2(\vec{r}-\vec{\Delta})^2]$ and the inverse of the spread of the wave function, α^{-1}, for an fcc structure of pure neutrons.

$10^{-15}\rho$ (g/cm^3)	α (fermi^{-1})	$l_{\max}$
1.83	2.924	4
3.34	3.597	5
4.4	3.937	6

$= V_c(^3P_2 - {}^3F_2)$.

Choice 2 (suggested by Bethe): In the singlet state, for the potential of the odd waves like the $^1P_1$ we take $V(^1P_1) = 6484.2e^{-7x}/x$ ($x = 0.7r$) the repulsive part of the singlet $^1S_0$ state. The triplet even waves like $V(^3S_1)$ and $V(^3D_j)$ were set equal to $V_c(^3P_2 - {}^3F_2)$. Likewise the $V(l_{\text{odd}} \geq 3)$ was set equal to $V_c(^3P_2 - {}^3F_2)$ as in choice 1.

Choice 3 (suggested by Bethe): All the undesired waves like $^1P_1$, $^1F_3$ from the singlet set and $^3S_1$, ^3D_j from the triplet sets were equated to the repulsive part of the singlet $^1S_0$, with the same prescription as in choices 1 and 2 for the potentials of the higher partial waves.

In the discussion of the results it will become clear from Table V (where the energy values obtained by using choices 2 and 3 are written above and below the results of choice 1) that choice 2 produces an energy about 25 MeV larger than choice 1, and similarly for choice 3.

An overriding concern in computations of this kind relates to the convergence of the many-body technique employed. Specifically, since the many-body method employed here considers only two-body correlations and since the density is rather high, there always remains the question regarding the validity of such a computation vis-à-vis the convergence of the series expansion of the interaction energy. Such a problem is unsolved in principle. We have already mentioned how the phenomenological form for the one-body wave function incorporates high-order correlations that are not present in the liquid plane waves. Besides, we have computed the "wound" parameter κ, whose size measures the importance of three-body correlations, and the result was ~0.2 at $\rho = 3.34\times10^{15}$ g/cm^3. In any event, for a crystal in which the particles are localized at lattice sites, it is rather improbable for three particles to come close enough to make the three-body contribution important. Lacking at the present time any systematic study of the value of the three-body effect in a quantum crystal in the framework of the t matrix, we can say that the rather small of κ is the only justification we can advance to believe that the cluster expansion here employed is actually convergent.[30]

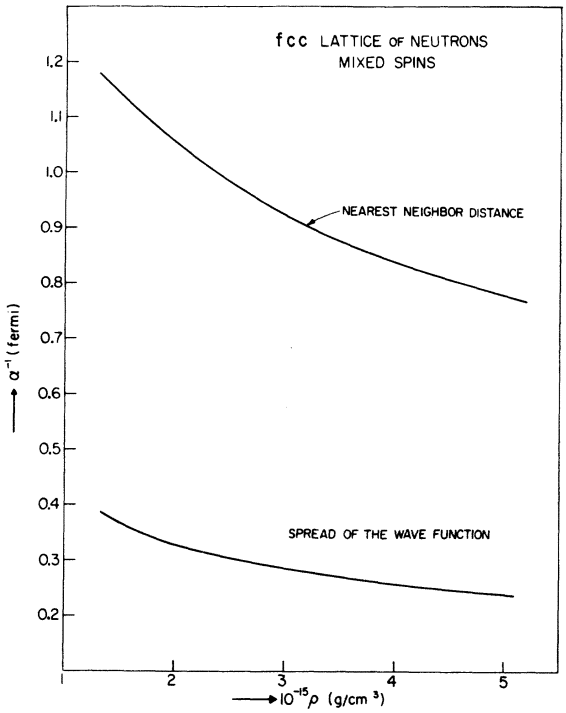

FIG. 3. The spread of the wave function, α^{-1} (fermi), as a function of the density, together with the nearest-neighbor distances for an fcc lattice of neutrons with mixed spins at a density of 3.34×10^{15} g/cm^3.

VIII. RESULTS AND COMPARISON WITH OTHER NEUTRON SOLID COMPUTATIONS

The geometrical configurations of the nucleons for fcc and bcc are respectively displayed in Figs.

TABLE II. For an fcc structure of pure neutrons with mixed spins the total energy per particle E/N (MeV) along with the potential energy and the kinetic energy as a function of the matter density $\rho = 4m/r_0^3$ (g/cm^3). The lattice constant r_0 is so defined that the nearest-neighbor distance is $r_0/\sqrt{2}$. We have inserted Kin. En. values up to 547 MeV even though at around 3.34×10^{15} g cm^{-3} one should already become worried about special-relativistic effects. After 3.33×10^{15} g cm^{-3} the numbers should therefore be taken with caution.

$10^{-15}\rho$ (g/cm^3)	r_0 (fermi)	Pot. En. (MeV)	Kin. En. (MeV)	E/N (MeV)
1.6	1.61	−110	250	140
1.83	1.54	−102	265	163
2.40	1.41	− 93	309	216
3.34	1.26	− 80	402	322
4.0	1.19	− 29	462	433
4.4	1.15	21	479	500
5.0	1.10	65	547	612

TABLE III. The spread of the wave function α^{-1} (fermi) determined self-consistently, the nearest-neighbor distance $\Delta = r_0/\sqrt{2}$ and the frequency of oscillation $\omega = \hbar\alpha^2/m$ ($\sec^{-1}$) as a function of the matter density ρ (g/cm^3). The localization parameter Λ is defined as the ratio of the available volume per particle ($\frac{1}{4}r_0^3$) and the actual volume occupied by the zero-point motion [$\frac{4}{3}\pi(2.5/\alpha^2)^{3/2}$], for an fcc lattice of neutrons.

$10^{-15}\rho$ (g/cm^3)	α^{-1}(self-consistent) (fermi)	Δ (fermi)	Λ	$10^{-24}\omega$ ($\sec^{-1}$)
1.83	0.342	1.089	1.379	5.382
2.4	0.312	0.995	1.391	6.468
3.34	0.278	0.891	1.415	8.146
4.0	0.259	0.839	1.456	9.385
4.40	0.254	0.817	1.491	9.759
5.0	0.238	0.779	1.501	11.115

1 and 2. We attempted a number of configurations to find, first of all, that on energetic grounds it is convenient to have only neutrons at high density; secondly, the fcc structure made up of neutrons with mixed spins does indeed appear to be the lowest energy configuration of pure neutron matter and the detailed results for such a configuration are displayed in Table II where the first column gives the density, the second the lattice constant, then the potential energy, followed by the kinetic energy [see discussion after Eq. (24)] and then finally the total energy. The spread of the wave function, as measured by α^{-1}(fermi), vs the density is exhibited in Fig. 3 along with the nearest-neighbor distance over the density range $1.6\times10^{15} \leq \rho \leq 5\times10^{15}$ g/cm^3. In Table III we list the density, the spread of the wave function α^{-1} determined self-consistently, the nearest-neighbor distance, the localization parameter Λ which is a measure of the ratio of the available volume per particle and the actual volume occupied by the zero-point motion of the particle, and the frequency of oscillation. It is evident that over the range of density of interest Λ is of the order 1.5. Such a small value of Λ is only to be expected for a highly quantum solidlike neutron lattice. The self-

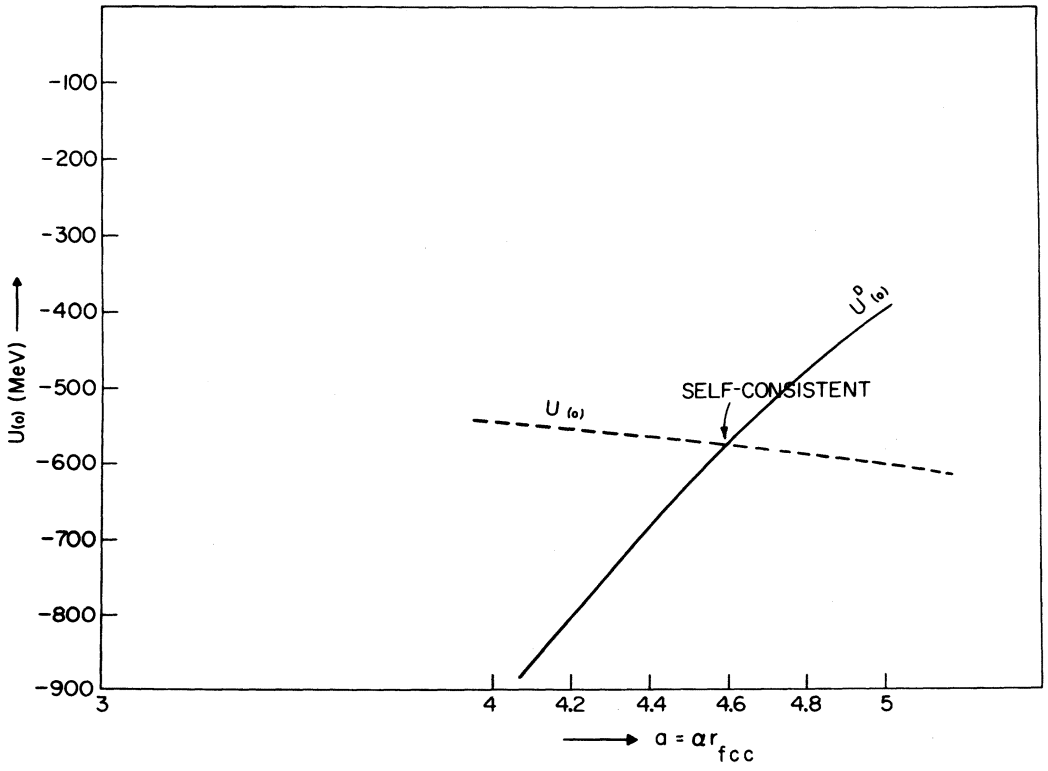

FIG. 4. The intersection of $U(0)$, determined by solving Eq. (34) and $U^D(0)$ yielded by Eq. (36) to localize the self-consistent value of α.

TABLE IV. Energy contribution per shell for an fcc structure of pure neutrons with mixed spins at a density of 1.83×10^{15} g/cm^3 and $r_0=1.54$ fermi together with the shell distances, Δ_k, the number of particles in each shell, n_k, and the cumulative potential-energy contribution, $\frac{1}{2}\sum_k n_k\epsilon_k$.

Δ_k (fermi)	n_k	$\frac{1}{2}(\epsilon_1+\epsilon_2)$ (MeV)	$\epsilon_2(\uparrow\downarrow)$ (MeV)	$\epsilon_1(\uparrow\uparrow)$ (MeV)	$\frac{1}{2}\sum_k n_k\epsilon_k$ (MeV)
1.089	12	5.84			35.04
1.540	6		−13.43		−3.25
1.886	24	−3.85			−51.45
2.177	12			0.58	−47.97
2.435	24	−1.35			−64.17
2.667	8		−2.18		−72.89
2.881	48	−0.59			−87.05
3.080	6			0.39	−85.88
3.267	36	−0.27			−89.66
3.443	24		−0.59		−96.74
3.611	24	−0.11			−98.06
3.771	24			0.23	−95.30

consistent α obtained by plotting $U(0)$ yielded by Eq. (34) and $U^D(0)$ determined by using Eq. (36) is indicated in Fig. 4 as the intersection of the two curves.

The detailed breakdown of energy contribution per shell (for the first 12 shells) for an fcc lattice with mixed spins for three densities ($\rho=1.83, 3.34, 4.4\times10^{15}$ g/cm^3) is shown in Tables IV, V, VI, and the shell contributions for $\rho=4.4\times10^{15}$ g/cm^3 are exhibited in Fig. 5 as a function of the shell distance (in fermi).

With a view to compare the energy obtained by using another configuration, we investigated a bcc lattice of neutrons with parallel spins at the density $\rho=3.34\times10^{15}$ g/cm^3 using choice 1 for the interaction potentials. The breakdown of the energy contribution per shell is displayed in Table VII. A similar breakdown for an fcc lattice of neutrons with mixed spins at the density $\rho=3.34\times10^{15}$g/cm^3 is displayed in Table V. It is instructive to compare the two results: at the same density a bcc lattice has the nearest and the next nearest neighbor, for example, at closer distances, thus picking up more repulsion as can be readily discerned from the numbers in Table VII. In the first shell there is a gain in energy with the bcc structure, but in the second and third shells the fcc structure is evidently energetically more favorable. Again,

TABLE V. Energy contribution per shell for an fcc structure of pure neutrons with mixed spins at a density of 3.34×10^{15} g/cm^3 and $r_0=1.2599$ fermi together with the shell distances, Δ_k, the number of particles in each shell, n_k, and the cumulative potential-energy contribution $\frac{1}{2}\sum_k n_k\epsilon_k$. The energy values in parentheses above and below are, respectively, those obtained with choices 2 and 3 for the interaction potentials.

Δ_k (fermi)	n_k	$\frac{1}{2}(\epsilon_1+\epsilon_2)$ (MeV)	$\epsilon_2(\uparrow\downarrow)$ (MeV)	$\epsilon_1(\uparrow\uparrow)$ (MeV)	$\frac{1}{2}\sum_k n_k\epsilon_k$ (MeV)
0.891	12	$27.40^{(34.49)}_{(31.18)}$			164.34
1.259	6		$-14.87^{(-14.98)}_{(-15.49)}$		119.73
1.543	24	$-6.41^{(-6.64)}_{(-6.68)}$			42.81
1.782	12			$1.45^{(1.39)}_{(1.38)}$	51.51
1.992	24	$-3.31^{(-3.31)}_{(-3.31)}$			11.79
2.182	8		−5.13		−8.73
2.357	48	−1.49			−44.49
2.519	6			0.52	−42.93
2.672	36	−0.75			−56.43
2.817	24		−1.51		−74.46
2.954	24	−0.38			−79.02
3.085	24			0.39	−74.34

in the fourth shell the bcc wins while in the fifth and sixth shells the fcc is more convenient and the pattern repeats until at the end one comes out with less energy (~25 MeV) on an fcc compared to a bcc. The difference may be considered marginal but nevertheless significant to favor an fcc structure with mixed spins for yielding the lowest energy configuration.

The plot of the energy per particle E/N vs density for neutron fluid[8] and fcc neutron solid is displayed in Fig. 6. We have indicated by error bars the changes in the values of the energy per particle with different choices for the interaction potentials. The difference brought about by these choices is at most ten percent; it may be noticed that at a given density the solid energies are lower than the fluid energies by as much as 25% at the high-density end. It is concluded that from density $\rho = 1.6\times10^{15}$ g/cm^3 upwards, the solidlike arrangement gives a lower energy per particle than the fluid. One can therefore say that it is convenient to have the neutron matter arranged in a lattice at ρ exceeding 1.6×10^{15} g/cm^3. It should be stressed that strictly speaking both solid and fluid energies should be calculated within the same methodological framework for a proper description of the fluid-solid transition. We have, however, compared our solid energies with Pandharipande's fluid energy[8] which has been computed variationally and as such it represents an upper bound. The present computation can, therefore, be regarded only as an indication for the onset of a solid phase at high density, but not a definite proof.

The energetic favorability of a neutron solid naturally raises the question of a phase change at high density and in order to determine the fluid-solid phase transition we perform a Maxwell construction using the previously quoted liquid energies which yields a solidification pressure of 2.1 $\times10^{35}$ dynes/cm^2 with a jump in the density from 1.6×10^{15} g/cm^3 (melting density) to 1.3×10^{15} g/cm^3 (crystallization density).

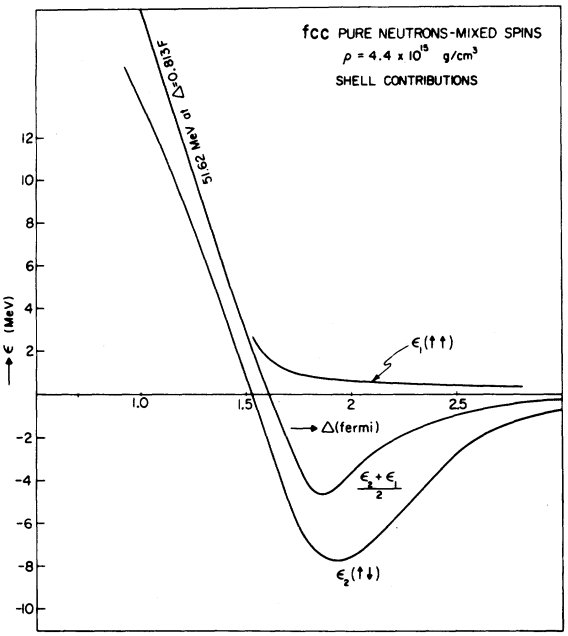

FIG. 5. Shell contribution in MeV as a function of the shell distances in fermi for fcc neutrons with mixed spins at $\rho = 4.4\times10^{15}$ g/cm^3.

Another interesting feature is the display of the elastic constants C_{11}, C_{12}, C_{44} shown in Table VIII as a function of the density: It can be seen that $C_{44} > 0$ for $\rho \simeq 1.6\times10^{15}$ g/cm^3, indicating that the fcc structure made up of neutrons can withstand the shearing stresses at a density upwards of this value and that it goes soft at about the same density where energetically the fluid phase is prefer-

TABLE VI. Energy contribution per shell for an fcc structure of pure neutrons with mixed spins at a density of 4.4×10^{15} g/cm^3 and $r_0 = 1.15$ fermi together with the shell distances, Δ_k, the number of particles in each shell, n_k, and the cumulative potential-energy contribution, $\frac{1}{2}\sum_k n_k \epsilon_k$.

Δ_k (fermi)	n_k	$\frac{1}{2}(\epsilon_1+\epsilon_2)$ (MeV)	$\epsilon_2(\uparrow\downarrow)$ (MeV)	$\epsilon_1(\uparrow\uparrow)$ (MeV)	$\frac{1}{2}\sum_k n_k \epsilon_k$ (MeV)
0.813	12	51.62			309.70
1.150	6		−10.25		279.00
1.408	24	5.34			214.92
1.626	12			1.29	222.66
1.818	24	−4.65			166.85
1.992	8		−7.06		138.61
2.151	48	−2.35			82.21
2.300	6			0.48	83.65
2.439	36	−1.20			62.05
2.571	24		−2.25		35.05
2.697	24	−0.65			27.25
2.816	24			0.40	32.05

TABLE VII. Energy contribution per shell for a bcc structure of pure neutrons with parallel spins at a density of 3.34×10^{15} g/cm^3 and $r_0=1.0005$ fermi together with the shell distances, Δ_k, the number of particles in each shell, n_k, and the cumulative potential-energy contribution, $\frac{1}{2}\sum_k n_k \epsilon_k$.

Δ_k (fermi)	n_k	$\epsilon_2(\uparrow\uparrow)$ (MeV)	$\epsilon_1(\uparrow\uparrow)$ (MeV)	$\frac{1}{2}\sum_k n_k \epsilon_k$ (MeV)
0.866	8	27.08		108.30
1.000	6		24.16	180.78
1.414	12		4.73	209.15
1.658	24	−13.90		42.45
1.732	8		1.58	48.76
2.000	6		0.91	51.50
2.179	24	−5.11		−9.80
2.236	24		0.68	−1.60
2.449	24		0.56	+5.08
2.598	32	−2.22		−30.43
2.828	12		0.39	−28.04
2.958	48	−1.18		−56.43

able to the solid phase. It may be argued that the "classical" approach of Born to compute the elastic constants may not be altogether adequate to take into account the contribution of phonons. Nevertheless, the values for C_{44} yielded by our quantum computations cannot be too far from reality.

We shall now discuss and compare the results of other neutron solid computations. To date there exist seven calculations to investigate the possibility of a neutron lattice at high density out of which six indicate the onset of a solid phase at some density between 4.2×10^{14} g/cm^3 and 3×10^{15} g/cm^3. These are displayed schematically in Fig. 7. The scaling arguments advanced by Anderson and Palmer[9] and Clark and Chao[10] can only be taken to provide a rough estimate of the solidification density. In the first instance their treatment is intened to yield only order of magnitude estimates and also the choice of the interaction potential is rather idealized. Nonetheless, their work does provide a positive answer to the question whether

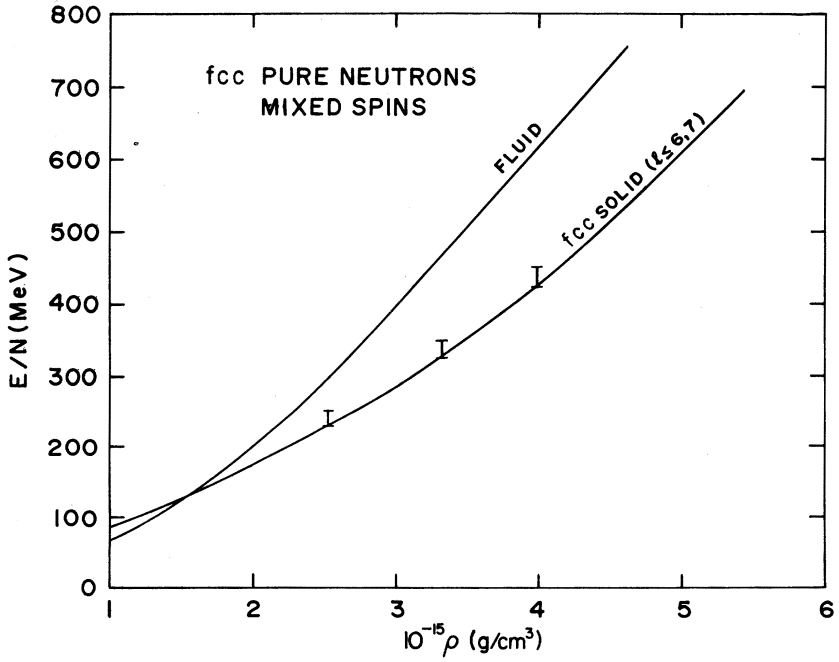

FIG. 6. Ground-state energy per particle vs the density for neutron fcc lattice. The neutron fluid is taken from Pandharipande (Ref.8). The error bars indicate the result with different choices for the unwanted waves in the interaction.

TABLE VIII. Elastic constants C_{11}, C_{12}, C_{44} in dynes/cm^2 for an fcc structure of pure neutrons with mixed spins against the matter density ρ.

$10^{-15}\rho$ (g/cm^3)	$10^{-36}C_{11}$ (dynes/cm^2)	$10^{-36}C_{12}$ (dynes/cm^2)	$10^{-36}C_{44}$ (dynes/cm^2)
5.0	27.57	10.33	5.71
4.4	17.59	6.69	3.43
4.0	13.15	4.98	2.52
3.34	6.78	2.97	1.47
2.4	2.65	1.07	0.48
1.83	0.89	0.37	0.09
1.6	0.40	0.24	0.03
1.4	0.16	0.15	−0.03

neutron matter would solidify under high enough pressure, and the approximate crystallization density comes out in the vicinity of 5×10^{14} g/cm^3. Coldwell[11] performs an Hartree-Fock calculation treating the degree of localization as a variational parameter to find that at a density of 7.78×10^{14} g/cm^3 the nucleons should be in a crystalline phase. The merit of this calculation is that it makes use of Mathieu functions as orthogonal single-particle wave functions: Such a wave function is capable of approximating either a gas or a crystal-like system depending on the value of a parameter present in the Mathieu functions. This choice enabled Coldwell to treat the nuclear gas and the nuclear crystal simultaneously and to set upper bounds to the energy resulting from a strictly Hartree-Fock calculation. An averaged two-body soft-core Reid potential was used in this computation and in that sense a complete state and angular momentum dependence was not taken into account. Schiff[13] determines the density and pressure at which neutrons will solidify by making use of a fermion analog of the quantum perturbation method developed by Kalos, Levesque, and Verlet and concluded that the main problem concerning dense neutron matter is not so much the many-body theory as the choice of the two-body interaction potential. An approximate choice for the neutron-neutron interaction potential gives a solidification density of $(2.9\pm0.5)\times10^{15}$ g/cm^3.

The Monte Carlo computation of Nosanow and Parish[12] treats the many-body clusters very satisfactorily, but the correlation function which in this formulation, was chosen to be $\exp[-(b/r)^n]$ with $n=4$. In Fig. 8 we have shown our correlated wave function ψ, the uncorrelated wave function φ along with the correlation function $f=\psi/\varphi$ for the singlet state $^1S_0$ for an fcc lattice of neutrons with mixed spins at $\rho=3.34\times10^{15}$ g/cm^3. The correlation functions of Pandharipande[14] and Nosanow and Parish[12] are shown in the same plot for comparison. It is evident from an inspection of the plots that the correlation function of Nosanow and Parish is rather different from the one obtained in the present work or by Pandharipande. The choice of $\exp[-(b/r)^4]$ forces f to be practically zero until a distance of 0.25 fermi and this will almost certainly reduce the contribution of the repulsive part of the interaction. Thus the choice of their f, even though justifiable at low density, becomes somewhat questionable as the density increases and the rather low solidification density obtained in their work is probably to be attributed to this particular form of the correlation function. The nucleon-

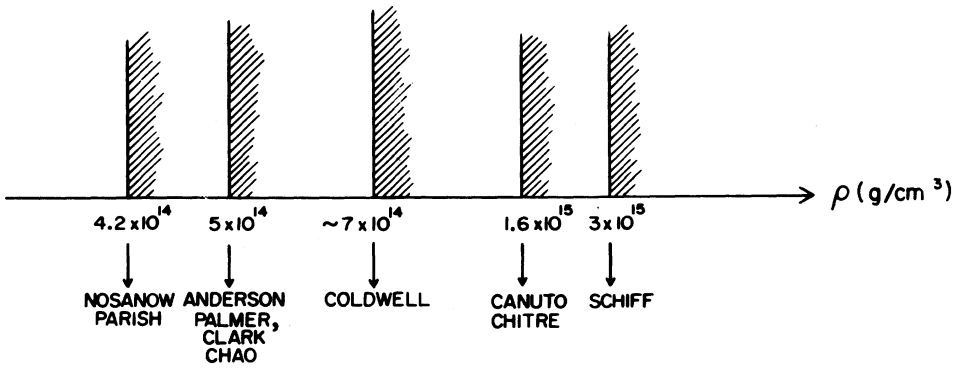

FIG. 7. Schematic representation of solidification density obtained by various neutron matter calculations.

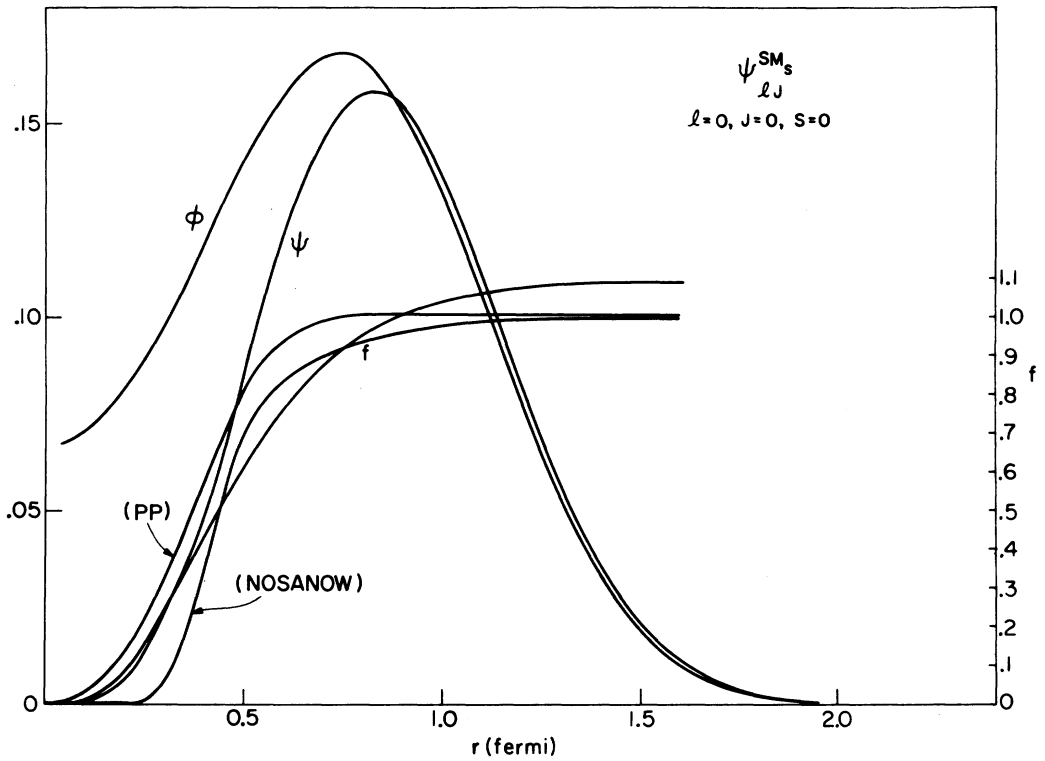

FIG. 8. The correlated wave function ψ, for the single-state $^1S_0$ along with the unperturbed wave function ϕ and the correlation function f, at $\rho = 3.34\times10^{15}$ g/cm^3 for the nearest-neighbor distance $\Delta = 0.891$ fermi. The correlation functions of Pandharipande (Ref. 14) and Nosanow (Ref. 12) are shown for comparison.

nucleon potential was also drastically simplified in order to make the Monte Carlo computation manageable.

In Pandharipande's work the variational calculation is supplemented by an equation satisfied by the correlation function f very similar to our Eq. (17). The point of departure arises when the important $\cos\theta$ term that couples odd and even waves is averaged and no angular momentum expansion of the wave function is performed, while in our formulation one of the major concerns is the state dependence of the correlation function which is exactly treated. The correlation function of Pandaripande never exceeds unity, but approaches it from below. Moreover, as can be seen from Fig. 8, his correlation function lifts very quickly near the origin probably because he constrains the f to heal at $d = 2r_0 - R_{\rm rms}$ (0.725 fermi at the density of 3.34×10^{15} g/cm^3), and as a result his f is always larger than our f for the most part when the potential is repulsive. There is another feature of Pandharipande's computation which seems to have more serious implications and this relates to his choice of the interaction potential. In our computation we take into account the full contribution of the noncentral forces wherever applicable, while Pandharipande assumes the central part of $V(^3P_2 - {}^3F_2)$ as the interaction uniformly for *all* the triplet states. We shall demonstrate that the final energy values are highly sensitive to the exact choice of the interaction potential.

We shall now compute the energy, using our formulation, for a bcc structure of neutrons with parallel spins at a density of 1.8 nucleons/fm^3 (or, $\rho = 3.01\times10^{15}$ g/cm^3) using the localization parameter and the potentials which Pandharipande[14] has used, viz. for the singlet state all the potentials were set equal to $V(^1D_2)$ and for the triplet states all the waves were taken to be given by $V_c(^3P_2 - {}^3F_2)$. With this prescription we were able to reproduce the energy of ~670 MeV which he obtains. A detailed break-down of energy for the first four shells is shown in Table IX. We believe taking just the central part of the $(^3P_2 - {}^3F_2)$ wave for all the triplet waves is a gross simplification of the interaction potential operating for the triplet states. This can be readily seen from Fig. 9 where we have shown the contributions of the central part of $^3P_2$ as well as the total $^3P_2$ wave. It is evident that there is a substantially attractive contribution from the LS component and as a result the effective $V(^3P_2) = V_c - \frac{2}{5}V_T + V_{LS}$ is largely attractive in the range of

TABLE IX. Energy contribution from the first four shells with our formulation and the following choice for interaction potential for a bcc structure of pure neutrons with parallel spins at a density of 3.01×10^{15} g/cm^3: all the singlet waves were set equal to $V(^1D_2)$ and all the triplet even waves were assumed to be given by $V_c(^3P_2)$, but the odd waves were taken from those given by Reid. The computation was repeated using Pandharipande's localization parameter and his choice of the potential viz. all the singlet waves $=V(^1D_2)$ and all the triplet waves $=V_c(^3P_2)$.

Δ_k (fermi)	n_k	$\epsilon_2(\uparrow\downarrow)$ (MeV)	$\epsilon_1(\uparrow\uparrow)$ (MeV)	$\epsilon_2(\uparrow\downarrow)$ (MeV)	$\epsilon_1(\uparrow\uparrow)$ (MeV)
0.866	8	47.35		57.13	
1.000	6		21.3		45.26
1.414	12		3.08		−2.06
1.658	24	−12.3		−8.56	
		$E/N\simeq 560$ MeV (present work)		$E/N\simeq 674$ MeV (Pandharipande)	
		$S=0$	$S=1$	$S=0$	$S=1$
		$V(^1D_2)$	Reid except $V(^3S_1)=V_c(^3P_2)$	$V(^1D_2)$	All waves $V_c(^3P_2)$

density of interest. We therefore repeated the computation for the bcc structure of neutrons with parallel spins at the same density using for the waves of the singlet state $V(^1D_2)$ and for the triplet state the undesired waves like $^3S_1$, were taken to be given by $V_C(^3P_2 - {}^3F_2)$, but elsewhere we use the full potentials given by Reid for each odd-wave explicitly. The result which is summarized in Table IX shows a drastic reduction in the energy of about 100 MeV over the value obtained by Pandharipande. Clearly one has to be extremely careful while handling the part of the problem concerning the interaction potential.

In order to ascertain the onset of solidification of a system one can for example compare the energies for the liquid and solid phases and determine which is lower. This demands that both energies be computed within the same many-body framework and with the same potentials. At the present time this is not possible for us to do, because we do not possess a value for the energy of the liquid computed with the t-matrix approach. Since we consider that the features of the spin and angular momentum dependence of $V(r)$ are very important features that can be accounted for in the solid in a fully satisfactory way with the t matrix, we concentrated our efforts in that direction.

Even though the comparison with Pandharipande's liquid is not fully justified, the drop in energy of the solid configuration is conspicuous enough to make room for possible uncettainties brought in by a different potential and many-body technique.

Finally, another way of looking at the phase transition is by considering the point (density) at which the mechanical stability of the crystal breaks down, indicating the onset of melting. Such a point, as discussed in Sec. VI and seen from Table VIII, is in excellent agreement with the value obtained by comparing the values of the energies.

IX. EQUATION OF STATE AND NEUTRON-STAR MODELS [3,15]

The equation of state derived by arranging neutrons with their spins mixed in an fcc lattice is summarized in Table X: Here in the first column

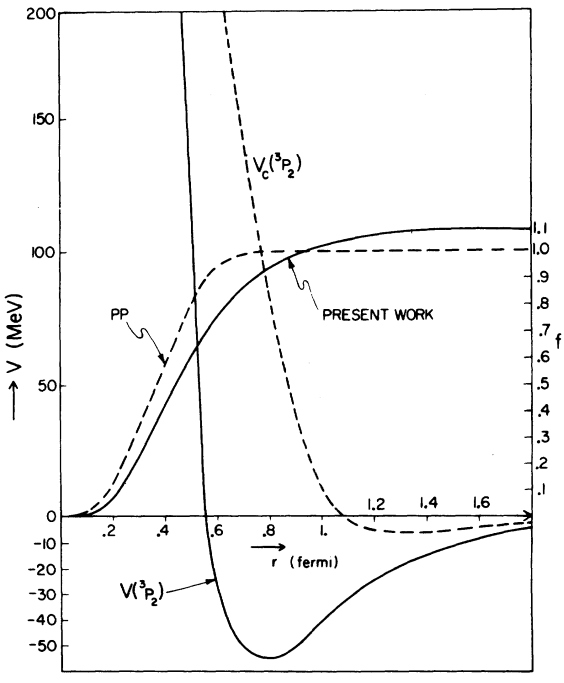

FIG. 9. The central part of $^3P_2$ wave and the total $^3P_2$ wave along with the correlation functions obtained in the present computation and by Pandharipande (Ref. 14).

TABLE X. Equation of state obtained with an fcc structure of pure neutrons with mixed spins: The first column shows the matter density ρ, the second the energy per particle, the third the mass-energy density ϵ, the fourth the pressure P, and lastly the adiabatic index $\Gamma = [(P+\epsilon)/\epsilon]\,(\partial P/\partial \epsilon)$.

$10^{-15}\rho$ (g/cm^3)	E/N (MeV)	$10^{-36}\epsilon$ (erg/cm^3)	$10^{-36}P$ (dynes/cm^2)	Γ
1.6	140	1.652	0.214	1.176
1.8	157	1.889	0.276	1.877
2.0	176	2.134	0.356	2.432
2.2	195	2.388	0.460	2.731
2.4	216	2.652	0.588	2.936
2.6	238	2.928	0.743	3.043
2.8	262	3.217	0.922	3.045
3.0	287	3.520	1.122	2.947
3.2	314	3.836	1.342	2.794
3.4	342	4.167	1.582	2.667
3.6	371	4.513	1.846	2.638
3.8	401	4.874	2.141	2.719
4.0	433	5.252	2.475	2.860
4.2	466	5.647	2.849	2.986
4.4	500	6.061	3.262	3.042
4.6	536	6.495	3.703	2.998
4.8	574	6.948	4.160	2.858
5.0	612	7.420	4.622	2.654

is a listing of the density (g/cm^3), the second lists the energy per particle (MeV), the third the mass-energy density ϵ (ergs/cm^3), the fourth the pressure derived by using the relation $P = -(\partial E/\partial V)$ and the last column gives the adiabatic index

$$\Gamma = \frac{P+\epsilon}{\epsilon}\,\frac{\partial P}{\partial \epsilon}.$$

The adiabatic index typically has values fluctuating above and below three at the high density end. It is the stiffness of the equation of state, characterized by these high values of Γ which is largely responsible for a flat density profile throughout much of the interior of a neutron star. We have fitted the pressure P vs the mass-energy density with a polynomial expression in the density range $1.6\times10^{15} \leq \rho \leq 6\times10^{15}$ g/cm^3

$$P_{36} = 0.20579 - 0.27160\,\epsilon_{36} + 0.181809\,\epsilon_{36}^{2} - 0.008037\,\epsilon_{36}^{3},$$

where

$$P_{36} = P\times10^{-36} \text{ dynes/cm}^2,$$

$$\epsilon_{36} = \epsilon\times10^{-36} \text{ ergs/cm}^3.$$

This is a useful formula which is likely to prove of help in the structure calculations.

To construct neutron-star models, we must solve the Tolman-Oppenheimer-Volkoff general-relativistic equations of stellar structure. The governing equations are

$$\frac{dP}{dr} = -\frac{G(\epsilon + P/c^2)(m + 4\pi r^3 P/c^2)}{r(r - 2Gm/c^2)},$$

$$\frac{dm}{dr} = 4\pi r^2 \epsilon,$$

where r is the radial coordinate, ϵ the mass-energy density, P the pressure, m the gravitational mass interior to radius r. In order to solve these equations to obtain the march of the physical variables inside a neutron star, we need to specify two boundary conditions $m(0) = 0$ and $\epsilon(0) = \epsilon_c$. These must be supplemented by the equation of state given by say, Baym, Pethick, and Sutherland[31] up to a density of the order of 1.3×10^{15} g/cm^3. This was continued by our equation of state *in the density range* $1.6\times10^{15} \leq \rho \leq 6\times10^{15}$ g/cm^3. In Table XI we list the central mass-energy density, the radius in kilometers and the mass in units of the solar mass and Fig. 10 exhibits a plot of $M/M_\odot$ vs ϵ_c. Our models are evidently in good agreement with those of Baym *et al.* up to a central mass-energy density of the order of 10^{15} g/cm^3; there is a departure at the high-density end because of the difference in the equation of state from the one employed by Baym *et al.* based on Pandharipande's pure neutron liquid calculation. We find a maximum mass of $1.39\,M_\odot$ for a stable neutron star at a central density of 5.2×10^{15} g/cm^3, not altogether different from a maximum mass of $1.66\,M_\odot$ calculated by Baym *et al.* at a central density of 4.1×10^{15} g/cm^3. Note from Table X that there is a remarkably little variation in the radius over most of the range of stable neutron-star masses. There is also a rapid decline in the mass-curve around a central mass-energy density of 10^{14} g/cm^3 which causes a very sharp

TABLE XI. Neutron-star models showing the radius in kilometers and the mass in units of solar mass as a function of the central mass-energy density.

ϵ_c (g/cm^3)	R (km)	$M/M_\odot$
8.293×10^{6}	4437	0.4762
6.589×10^{7}	3549	0.8242
3.304×10^{8}	2648	0.9777
1.045×10^{9}	2069	1.0018
2.626×10^{9}	1732	0.9598
8.312×10^{9}	1283	0.9073
1.659×10^{10}	1055	0.8744
3.313×10^{10}	879	0.8436
6.617×10^{10}	736	0.8029
1.322×10^{11}	597	0.7563
4.188×10^{11}	469	0.677
9.728×10^{11}	466	0.660
3.833×10^{12}	518	0.635
7.801×10^{12}	577	0.623
1.340×10^{13}	669	0.614
2.68×10^{13}	851	0.611
4.56×10^{13}	1134	0.612
8.83×10^{13}	2173	0.615
1.801×10^{14}	54.5	0.101
2.772×10^{14}	25.5	0.122
4.166×10^{14}	16.1	0.158
7.978×10^{14}	9.9	0.668
1.651×10^{15}	9.634	1.1157
1.883×10^{15}	9.453	1.1158
2.121×10^{15}	9.243	1.1968
2.376×10^{15}	9.014	1.2353
2.631×10^{15}	8.760	1.2690
2.912×10^{15}	8.516	1.3003
3.198×10^{15}	8.300	1.3278
3.498×10^{15}	8.101	1.3490
3.829×10^{15}	7.929	1.3649
4.161×10^{15}	7.770	1.3755
4.503×10^{15}	7.618	1.3824
5.232×10^{15}	7.351	1.3873
6.042×10^{15}	7.095	1.3824
6.466×10^{15}	6.986	1.3779
7.411×10^{15}	6.794	1.3655

decrease in the radius of the star. The curve begins to rise in the region of stable neutron stars up to a central mass-energy density of 5.2×10^{15} g/cm^3 where the radius of the neutron star at the maximum is about twice the Schwarzschild radius and as a result general relativistic effects overwhelm the stability of the model upwards of the density of 5.2×10^{15} g/cm^3 causing a decline of the mass-ϵ_c curve shown in Fig. 10.

Finally, we might say that the theoretical computations indicate that there is a very good chance for neutron matter to solidify at very high density, but the proof for such a proposition has to come from astrophysical considerations. There is indeed one piece of observational evidence which lends credence to the idea of a solid core inside heavy neutron stars. This pertains to the fact that the starquake theory of pulsar speed-ups and the subsequent healing which has been so successfully applied to account for the Crab pulsar, can explain the observational features associated with the Vela pulsar only if it is assumed that the latter possesses a solid core. Pines, Shaham, and Ruderman[32] have made convincing arguments to explain the significant Vela pulsar speed-ups as arising from core-quakes suddenly releasing the elastic energy stored in the inner, solid neutron lattice. This is due to the fact that the shear modulus of the core is some five orders of magnitude larger than that of the crust and as a result the core has sufficient elastic energy "to power the starquakes of this magnitude ($\Delta\Omega/\Omega\sim10^{-6}$) and frequency (every few years)." The presence of a solid core also substantially reduces the ratio of the superfluid moment of inertia to that of the rest of the star and this feature is in accord with the observed structure factor for Vela. In conclusion we could say that the speed-ups observed in pulsars have distinctly contributed in shifting the idea of a solid core inside a heavy neutron star to the plausible end of the credibility spectrum.

X. OPEN PROBLEMS

Now that the results have been presented, it is necessary to consider in which directions the present computation has to be improved. First of all, the Hamiltonian (12) does not possess the right properties under parity inversion, $\vec{r}\to-\vec{r}$. This

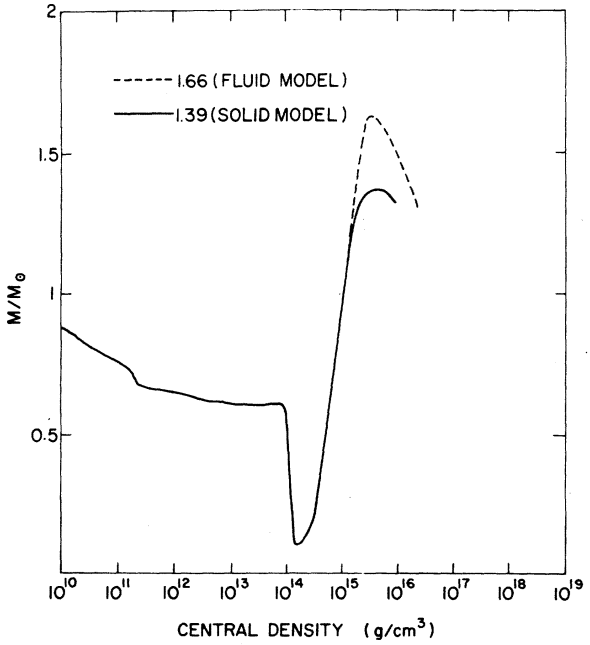

FIG. 10. Neutron-star mass in units of the solar mass vs the central mass-energy density (g/cm^3). The dashed curve is from Baym *et al.* (Ref. 31).

comes about from using, for $U(1)$ and $U(2)$, simple harmonic oscillator potentials located at the two different lattice sites. In every equation except the B-G equation we have employed antisymmetrized ψ's, i.e., both in the energy expressions [Eq. (26)] and in the determination of $U(0)$ [Eq. (34)].

The unwanted waves like $^1P_1$, $^3S_1$, etc., however, make their presence felt dynamically through the parity nonconserving B-G equations. This peculiar behavior has to be modified in such a way that only the appropriate waves enter both in the energy and the dynamic equation.

Second, the treatment of the noncentral forces, especially the tensor force, requires special care. In a liquid at high density such a force has no great effect and one could stretch the argument and suppose that this is also true for a quantum crystal. However, this statement can be proven only by an explicit computation. An exact computation would require that the angle between $\vec{r}$ and $\vec{\Delta}$ that enters in the new parity-invariant Hamiltonian has to be understood as

$$\cos\gamma = \cos\theta_1 \cos\theta_2 + \sin\theta_1 \sin\theta_2 \cos(\varphi_1 - \varphi_2),$$

where (θ_1, φ_1) refer, say, to $\vec{r}$ and (θ_2, φ_2) to $\vec{\Delta}$. The angles (θ_2, φ_2) are given by the crystallographic position of the distinct lattice points, i.e., the direction cosines have to be specified. With such a complicated geometry the B-G equation is extremely difficult to analyze and the authors think that it is worth doing it only when a parity-conserving Hamiltonian has been found. As we said earlier, this exact geometrical treatment would ensure a thoroughly correct account of the tensor force which is however mostly contributed by one-boson exchange potential (OBEP). This contribution is known to be relatively unimportant at high density and one has therefore to weigh carefully the gain obtained by such a complicated treatment against the importance of tensor forces at high density. Their importance cannot be totally ascertained at the present time since the Bethe-Johnston potential has not yet been developed and no definite statement can be made regarding its tensor component. All these problems are under study and the results will be communicated elsewhere.

APPENDIX: NUMERICAL METHOD

We shall present a symmary of the numerical method employed to solve the three sets of Eqs. (22). The principal problem is to obtain both the eigenvalues and the corresponding eigenfunctions numerically; in particular, we are interested in locating the lowest eigenvalue and its eigenfunction. Each set in (22) contains a certain number of coupled second-order linear differential equations satisfied by functions F, G, H with the boundary conditions that the functions vanish at the origin and at infinity. This is clearly an eigenvalue problem, for the solution of which we proceed in two steps. First we reduce the problem to obtaining the solution of a set of linear equations which is also an eigenvalue problem for a matrix. Secondly, we use a numerical method for finding the lowest eigenvalue of the matrix and its eigenvector. This method, which is known as the power method, is used extensively in numerical analysis and is briefly reviewed here.

Assume that an arbitrary n-dimensional vector $\vec{X}$ can be expanded in terms of the eigenvectors of a matrix A, i.e., write

$$\vec{X} = c_1\vec{U}_1 + c_2\vec{U}_2 + \cdots + c_n\vec{U}_n,$$

where $\vec{U}_j$ is the eigenvector corresponding to the eigenvalue λ_j, i.e., $A\vec{U}_j = \lambda_j\vec{U}_j$, and for definiteness we arrange the eigenvalues in a descending order, $\lambda_1 \geq \lambda_2 \geq \lambda_3 \geq \cdots \geq \lambda_n$.

We then have

$$A\vec{X} = c_1A\vec{U}_1 + c_2A\vec{U}_2 + \cdots + c_nA\vec{U}_n$$
$$= c_1\lambda_1\vec{U}_1 + c_2\lambda_2\vec{U}_2 + \cdots + c_n\lambda_n\vec{U}_n.$$

Repeating the procedure k times, we have

$$A^k\vec{X} = c_1\lambda_1{}^k\vec{U}_1 + \cdots + c_j\lambda_j{}^k\vec{U}_j + \cdots + c_n\lambda_n{}^k\vec{U}_n.$$

This is a power series with the term with the largest (in absolute value) eigenvalue dominating the series.

A similar argument can be made for the inverse of the matrix A to get

$$A^{-1}\vec{X} = c_1\lambda_1{}^{-1}\vec{U}_1 + c_2\lambda_2{}^{-1}\vec{U}_2 + \cdots + c_n\lambda_n{}^{-1}\vec{U}_n$$

and in general

$$(A^{-1})^k\vec{X} = c_1\lambda_1{}^{-k}\vec{U}_1 + c_2\lambda_2{}^{-k}\vec{U}_2 + \cdots + c_n\lambda_n{}^{-k}\vec{U}_n.$$

In this power series expansion the smallest (in aboslute value) eigenvalue would evidently dominate. If we now subtract a constant, say λ_0, times the identity matrix I from the matrix A, then the eigenvalues of the matrix $(A-\lambda_0 I)$ are clearly $(\lambda_j - \lambda_0)$ $(j = 1, 2, \ldots n)$ and those of the inverse $(A-\lambda_0 I)^{-1}$ are $(\lambda_j - \lambda_0)^{-1}$ $(j = 1, 2, \ldots n)$ with the corresponding eigenvectors $\vec{U}_j$. Taking powers of $(A-\lambda_0 I)^{-1}$ applied to an arbitrary vector $\vec{X}$ which can be expanded in terms of the eigenvectors $\vec{U}_j$, we get

$$(A-\lambda_0 I)^{-k}\vec{X} = c_1(\lambda_1-\lambda_0)^{-k}\vec{U}_1 + \cdots$$
$$+ c_j(\lambda_j-\lambda_0)^{-k}\vec{U}_j + \cdots$$
$$+ c_n(\lambda_n-\lambda_0)^{-k}\vec{U}_n.$$

We shall call the constant λ_0 the shift of the eigen-

values and clearly in the power-series expansion for sufficiently large k the term which dominates is the one with the eigenvalue closest to the shift λ_0, i.e., if λ_j is the smallest eigenvalue and $\lambda_0 < \lambda_j$, the series converges to

$$(A-\lambda_0 I)^{-k}\vec{X} = \frac{c_j \vec{U}_j}{(\lambda_j-\lambda_0)^k},$$

λ_j is then given by

$$\lambda_j = \lambda_0 + \frac{(A-\lambda_0 I)^{-k}\vec{X}}{(A-\lambda_0 I)^{-(k+1)}\vec{X}}$$

and

$$\vec{U}_j \sim (A-\lambda_0 I)^{-k}\vec{X}.$$

We thus have a method of arriving at the lowest eigenvalue which involves choice of λ_0 of various depths to find the eigenvalue closest to it in each case. Should the computation yield the same eigenvalue repeatedly, one may reasonably conclude that the lowest eigenvalue has been obtained.

We shall illustrate the method by explicitly showing how it applies to the first set of equations in (22) which when written in full give:

$$F_0'' + (E-U_0)F_0 + a(x,d)F_1 = 0,$$

$$F_1'' + (E-U_1)F_1 + \tfrac{1}{3}a(x,d)(F_0 - 2F_2) = 0,$$

$$F_2'' + (E-U_2)F_2 - \tfrac{1}{5}a(x,d)(2F_1 - 3F_3) = 0,$$

$$F_3'' + (E-U_3)F_3 + \tfrac{1}{7}a(x,d)(3F_2 - 4F_4) = 0,$$

$$F_4'' + (E-U_4)F_4 - \tfrac{1}{9}a(x,d)(4F_3 - 5F_5) = 0,$$

$$F_5'' + (E-U_5) + \tfrac{1}{11}a(x,d)(5F_4 - 6F_6) = 0,$$

$$F_6'' + (E-U_6) - \tfrac{1}{13}a(x,d)(6F_5) = 0\ .$$

If we apply central differences to this set of equations we have at the ith point (with $k = x^{i+1} - x^i$):

$$\frac{F_0^{i+1} - 2F_0^i + F_0^{i-1}}{k^2} - U_0 F_0^i + a(x,d)F_1^i = -EF_0^i,$$

$$\frac{F_1^{i+1} - 2F_1^i + F_1^{i-1}}{k^2} - U_1 F_1^i + \frac{a(x,d)}{3}(F_0^i - 2F_2^i) = -EF_1^i,$$

$$\frac{F_2^{i+1} - 2F_2^i + F_2^{i-1}}{k^2} - U_2 F_2^i - \frac{a(x,d)}{5}(2F_1^i - 3F_3^i) = -EF_2^i,$$

$$\cdots,$$

$$\frac{F_6^{i+1} - 2F_6^i + F_6^{i-1}}{k^2} - U_6 F_6^i - \frac{a(x,d)}{13}(6F_5^i) = -EF_6^i\ .$$

Here $F_0^i = F_0(x^i)$, $F_1^i = F_1(x^i)$, etc. and $1 \leqslant i \leqslant (N-2)$, N being the number of points in the interval; $i = 1$ is the point next to the left end-point and $i = N-2$ is the corresponding point next to the right-hand end point. The zero boundary conditions at the end points evidently demand that F^{i-1} and F^{i+1} vanish at those points.

Let us consider a vector $\vec{U}$ made up of blocks of elements when the ith block consists of the set $(F_0^i, F_1^i, F_2^i, F_3^i, F_4^i, F_5^i, F_6^i)$. Then the equations may be cast in the form of a matrix equation

$$A\vec{U} = -k^2 E\vec{U},$$

where

$$A = \begin{bmatrix} [K_1][I] & 0 & 0 & \cdots & 0 \\ 0 & [I][K_2][I] & 0 & \cdots & 0 \\ 0 & 0 & [I][K_3][I] & \cdots & 0 \\ \cdot & \cdot & \cdot & \cdot & \cdot \\ \cdot & \cdot & \cdot & \cdot & \cdot \\ \cdot & \cdot & \cdot & \cdot & \cdot \\ 0 & 0 & 0 & \cdots & [I][K_n] \end{bmatrix}, \qquad \vec{U} = \begin{bmatrix} F_0^1 \\ F_1^1 \\ F_2^1 \\ \cdot \\ \cdot \\ \cdot \\ F_0^{N-2} \\ F_1^{N-2} \\ \cdot \\ \cdot \\ \cdot \\ F_6^{N-2} \end{bmatrix},$$

$$I = \begin{bmatrix} 1 & & & & & & \\ & 1 & & 0 & & & \\ & & 1 & & & & \\ & & & 1 & & & \\ & 0 & & & 1 & & \\ & & & & & 1 & \\ & & & & & & 1 \end{bmatrix},$$

$$K = \begin{bmatrix} -2-k^2U_0 & a(x,d)k^2 & 0 & 0 & 0 & 0 & 0 \\ -\frac{1}{3}a(x,d)k^2 & -2-k^2U_1 & -\frac{2}{3}a(x,d)k^2 & 0 & 0 & 0 & 0 \\ 0 & -\frac{2}{5}a(x,d)k^2 & -2-k^2U_2 & \frac{3}{5}a(x,d)k^2 & 0 & 0 & 0 \\ 0 & 0 & -\frac{3}{7}a(x,d)k^2 & -2-k^2U_3 & -\frac{4}{7}a(x,d)k^2 & 0 & 0 \\ 0 & 0 & 0 & -\frac{4}{9}a(x,d)k^2 & -2-k^2U_4 & \frac{5}{9}a(x,d)k^2 & 0 \\ 0 & 0 & 0 & 0 & \frac{5}{11}a(x,d)k^2 & -2-k^2U_5 & -\frac{6}{11}a(x,d)k^2 \\ 0 & 0 & 0 & 0 & 0 & -\frac{6}{13}a(x,d)k^2 & -2-k^2U_6 \end{bmatrix}.$$

The above formulation can be extended to any number of equations and the power method can be used to look for the lowest eigenvalue for this matrix equation.

ACKNOWLEDGMENTS

It is a pleasure to thank Dr. H. A. Bethe, Dr. B. Brandow, Dr. A.G.W. Cameron, Dr. L. Nosanow, Dr. V. R. Pandharipande, and Dr. M.A. Ruderman for their continued interest and helpful criticism. One of us (S.M.C.) would like to express his gratitude to Dr. R. Jastrow for his hospitality at the Institute for Space Studies, New York.

*Also with the Department of Physics, City College of the City University of New York, New York.

†On leave of absence from the Tata Institute of Fundamental Research, Bombay, India.

[1]J. A. Wheeler, Annu. Rev. Astron. Astrophys. 4, 393 (1966).

[2]A. G. W. Cameron, Annu. Rev. Astron. Astrophys. 8, 179 (1970).

[3]V. Canuto, Annu. Rev. Astron. Astrophys. (to be published).

[4]M. A. Ruderman, Annu. Rev. Astron. Astrophys. 10, 427 (1972).

[5]J. R. Oppenheimer and G. M. Volkoff, Phys. Rev. 55, 374 (1939).

[6]S. Tsuruta and A. G. W. Cameron, Can. J. Phys. 43, 2056 (1965).

[7]B. Banerjee, S. M. Chitre and V. K. Garde, Phys. Rev. Lett. 25, 1125 (1970).

[8]V. R. Pandharipande, Nucl. Phys. A174, 641 (1971).

[9]P. W. Anderson and R. G. Palmer, Nat. Phys. Sci. 231, 145 (1971).

[10]J. W. Clark and N. C. Chao, Nat. Phys. Sci. 236, 37 (1972).

[11]R. L. Coldwell, Phys. Rev. D 5, 1273 (1972).

[12]L. H. Nosanow and L. J. Parish (private communication).

[13]D. Schiff, Nature (Lond.) 243, 130 (1973).

[14]V. R. Pandharipande (private communication).

[15]V. Canuto and S. M. Chitre, Phys. Rev. Lett. 30, 999 (1973); Nature (Lond.) 243, 63 (1973).

[16]B. H. Brandow, Ann. Phys. (N.Y.) 74, 112 (1972).

[17]R. A. Guyer, *Solid State Physics*, edited by F. Seitz, D. Turnbull, and H. Ehrenreich (Academic, New York, 1969), Vol. 23, p. 413.

[18]L. H. Nosanow, Phys. Rev. 146, 120 (1966).

[19]J. P. Hansen and D. Levesque, Phys. Rev. 165, 293 (1968).

[20]W. E. Massey and C. W. Woo, Phys. Rev. 165, 293 (1968).

[21]F. J. Iwamoto and H. Namaizawa, Prog. Theor. Phys. Suppl. 37 and 38, 234 (1966).

[22]R. A. Guyer and L. I. Zane, Phys. Rev. 188, 445 (1969).

[23]B. Sarkissian, Ph.D. thesis, Duke University, 1969 (unpublished).

[24]H. Horner, Phys. Rev. A 1, 1712 (1970); 1, 1722 (1970).

[25]C. Ebner and C. C. Sung, Phys. Rev. A 4, 269 (1971).

[26]E. Østgaard, J. Low Temp. Phys. 8, 479 (1972).
[27]H. A. Bethe, B. H. Brandow, and A. G. Petschek, Phys. Rev. 129, 225 (1963).
[28]M. Born, Proc. Camb. Phil. Soc. 36, 160 (1940).
[29]B. H. Brandow (private communication).
[30]V. Canuto, J. Lodenquai, and S. M. Chitre, Phys. Rev. A 8, 949 (1973).
[31]G. Baym, C. Pethick, and P. Sutherland, Astrophys. J. 170, 299 (1971).
[32]D. Pines, J. Shaham, and M. Ruderman, Nature (Lond.) 237, 83 (1972).

PHYSICAL REVIEW D VOLUME 9, NUMBER 6 15 MARCH 1974

Energy of neutron-star matter*

Steven A. Moszkowski
University of California, Los Angeles, California 90024
(Received 30 August 1973)

It is generally believed that the interior of some neutron stars is dense enough that the neutron-star matter (NSM) contains not only neutrons, but also protons, electrons, and various hyperons. In the present paper we calculate the effect of some hyperons on the composition and energy of the NSM. We calculate the energy per baryon and the fractions of the various baryons present, as a function of the baryon density, ranging from 0.1 to 2 baryons per fm^3, using two slightly different modifications of the Reid–soft-core interaction, one developed by Sawada and Wong, and the other by Campi and Sprung. The interaction energies are based on reaction matrix calculations by the above authors. We consider first a pure neutron gas. However, even at subnuclear densities (≤ 0.15 baryons per fm^3) it is generally agreed that there are protons present (and also electrons to keep the system neutral.) We calculate the effect of the protons (which constitute less than 10% of the baryons) on the energy. We then study the effect of what, we believe, are the most important hyperons, namely, Σ^-, Λ, Δ^-, to the composition and energy. The baryon-baryon interaction energies are assumed to be essentially the same as those between nucleons, except that (1) the interaction energy is different between like baryons ($\Lambda\Lambda$ or pp) and unlike baryons ($\Lambda\Sigma^-$ or np); and (2) there is a special factor of $\frac{2}{3}$ in the strengths of the long-range attractive part of the hyperon-nucleon interaction, as compared to the nucleon-nucleon interaction. The latter is argued on the basis of a quark model. On the other hand, the short-range repulsive part of the interaction is assumed to be the same between all baryon pairs. Four different models are used. One of our main conclusions is that, in the most realistic of the four models used here, there are relatively few protons and hyperons present (no more than 15% of each species even at the highest density considered) and the energy is only slightly less than for a pure neutron gas (20% and 10%, respectively, for the Sawada-Wong and Campi-Sprung interactions). Finally, we calculate the magnetic susceptibility of NSM treated as a pure neutron gas with Sawada-Wong interaction energies. No evidence of a transition to ferromagnetism is found.

INTRODUCTION

Neutron stars have been a subject of great interest for many years, but especially since the discovery of pulsars in 1967. An important aspect in determining the stability of neutron stars is the equation of state (EOS) relating the pressure to the density. Thus for different EOS used, one obtains a maximum gravitational neutron-star mass up to about 2 solar masses.[1] In order to discuss the EOS we need some model of neutron-star matter (NSM). The EOS up to about normal nuclear matter density (2.7×10^{14} g/cm^3 or 0.16 nucleons per fm^3) is now quite well understood. At densities above about 10^{14} g/cm^3, NSM is believed to be made up of neutrons, protons, and electrons[2] (together with a few muons). At even higher densities, hyperons appear.[3] Their presence is, however, quite sensitive to the interactions among hyperons and nucleons.

The properties of NSM including hyperons have been studied previously by, for example, neglecting all interactions and taking only the kinetic energies of the baryons (and electrons) into account.[1,4] More recently, Tsuruta and Cameron[3] and also Langer and Rosen[5] considered the prop-